
Spatial Factor Modeling: A Bayesian Matrix-Normal Approach for Misaligned Data

LU ZHANG

UCLA DEPARTMENT OF BIostatISTICS

Lu.Zhang@ucla.edu

SUDIPTO BANERJEE

UCLA DEPARTMENT OF BIostatISTICS

sudipto@ucla.edu

May 25, 2022

Abstract

Multivariate spatially-oriented data sets are prevalent in the environmental and physical sciences. Scientists seek to jointly model multiple variables, each indexed by a spatial location, to capture any underlying spatial association for each variable and associations among the different dependent variables. Multivariate latent spatial process models have proved effective in driving statistical inference and rendering better predictive inference at arbitrary locations for the spatial process. High-dimensional multivariate spatial data, which is the theme of this article, refers to data sets where the number of spatial locations and the number of spatially dependent variables is very large. The field has witnessed substantial developments in scalable models for univariate spatial processes, but such methods for multivariate spatial processes, especially when the number of outcomes is moderately large, are limited in comparison. Here, we extend scalable modeling strategies for a single process to multivariate processes. We pursue Bayesian inference which is attractive for full uncertainty quantification of the latent spatial process. Our approach exploits distribution theory for the Matrix-Normal distribution, which we use to construct scalable versions of a hierarchical linear model of coregionalization (LMC) and spatial factor models that deliver inference over a high-dimensional parameter space including the latent spatial process. We illustrate the computational and inferential benefits of our algorithms over competing methods using simulation studies and an analysis of a massive vegetation index dataset.

Key words: Bayesian inference; Factor models; Linear Models of Coregionalization; Matrix-Normal distribution; Multivariate spatial processes; Scalable spatial modeling

I. INTRODUCTION

This manuscript develops a new class of hierarchical models for analyzing multiple spatially oriented variables in high-dimensional settings. Multivariate spatial models are typically driven by vector-valued latent spatial stochastic processes, such as a multivariate Gaussian process, to capture the spatial dependence for each variable while also accounting for associations among each variable (see, e.g., Cressie, 1993; Chilés and Delfiner, 1999; Wackernagel, 2003; Gelfand and Banerjee, 2010; Cressie and Wikle, 2015, and references therein). Multivariate spatial processes are specified with matrix-valued cross-covariance functions (see, e.g., Genton and Kleiber, 2015; Salvaña and Genton, 2020; Le and Zidek, 2006, and references therein) to model associations among the multiple variables at any two spatial locations. Theoretical characterizations of cross-covariances are well established, but practical modeling implications and computational efficiency require specific considerations depending upon the application (see, e.g. Brown et al., 1994; Le et al., 1997; Sun et al., 1998; Le et al., 2001; Gamerman and Moreira, 2004; Schmidt and Gelfand, 2003; Banerjee et al., 2014, and references therein).

We address multivariate spatial modeling in high-dimensional settings dealing with a potentially large number of dependent variables over a massive number of locations. While analyzing massive spatial and spatial-temporal databases have received much attention (see, e.g., Sun et al., 2011; Banerjee, 2017; Heaton et al., 2019; Zhang et al., 2020, and references therein for an account of the expanding literature in this domain), the bulk of these methods have focused on one or very few (two or three) spatially dependent variables and often have to rely upon restrictive assumptions that preclude full inference on the latent process. With larger numbers of dependent variables, modeling the cross-covariance becomes challenging. Even for stationary cross-covariance functions, where we assume that the associations among the variables do not change over space and the spatial association for each variable depends only on the translation vector connecting two locations, matters become computationally challenging.

The scalable modeling approach we develop here enriches the popular linear models of coregionalization (Bourgault and Marcotte, 1991; Wackernagel, 2003; Gelfand et al., 2004; Chiles and Delfiner, 2009; Genton and Kleiber, 2015) using a Matrix-Normal distribution to model the linear transformation on latent spatial processes. Our contribution extends existing classes of spatial factor models by offering fully model-based analysis of spatial misalignment, where not all responses are recorded over the same set of locations. The literature in this context is comparatively sparse for large datasets. Spatial factor models have been explored in different contexts including by Wang and Wall (2003), Lopes et al. (2008), Ren and Banerjee (2013) and Taylor-Rodriguez et al. (2019). An extensive discussion on how hierarchical models emerged from dynamic factor models is found in Lopes et al. (2008) and references therein. Ren and Banerjee (2013) proposed low-rank specifications for spatially-varying factors to achieve dimension reduction in number of locations and variables, but such low-rank specifications tend to over-smooth the latent process from massive data sets containing millions of locations. More recently, Taylor-Rodriguez et al. (2019) consider Nearest-Neighbor Gaussian process (Datta et al., 2016a) for spatial factors with the usual constrained loading matrices in non-spatial factor models. These are more restrictive than needed for identifying spatially correlated factors (see, e.g. Ren and Banerjee, 2013).

In the next section, we collect some results in multivariate geostatistical modeling. We develop our modeling framework in Section II. In Section III, we state some theoretical results about posterior consistency for the proposed models. Simulation studies for exploring the performance of proposed models are summarized in Section IV. An analysis illustrating our methods is presented in Section V. We conclude with some discussion in Section VI.

II. MULTIVARIATE SPATIAL PROCESSES

Let $\mathbf{z}(\mathbf{s}) = (z_1(\mathbf{s}), \dots, z_q(\mathbf{s}))^\top$ be a $q \times 1$ stochastic process, where each $z_i(\mathbf{s})$ is a real-valued random variable at location $\mathbf{s} \in \mathcal{D} \subseteq \mathbb{R}^d$. The process is specified by its mean $E[z_i(\mathbf{s})] = \mu_i(\mathbf{s})$ and, customarily, second-order stationary covariances $C_{ij}(\mathbf{h}) = \text{Cov}\{z_i(\mathbf{s}), z_j(\mathbf{s} + \mathbf{h})\}$ for $i, j = 1, 2, \dots, q$. These covariances define the matrix-valued $q \times q$ cross-covariance function $\mathbf{C}(\mathbf{h}) = \{C_{ij}(\mathbf{h})\}$ with (i, j) -th entry $C_{ij}(\mathbf{h})$. While there is no loss of generality in assuming the process mean to be zero by absorbing the mean into a separate regression component in the model, as we will do here, modeling the cross-covariance function requires care. From its definition, $\mathbf{C}(\mathbf{h})$ need not be symmetric, but must satisfy $\mathbf{C}(\mathbf{h})^\top = \mathbf{C}(-\mathbf{h})$. Also, since $\text{var}\{\sum_{i=1}^n \mathbf{a}_i^\top \mathbf{z}(\mathbf{s}_i)\} \geq 0$ for any set of finite locations $\mathbf{s}_1, \mathbf{s}_2, \dots, \mathbf{s}_n \in \mathcal{D}$ and any set of constant vectors $\mathbf{a}_1, \mathbf{a}_2, \dots, \mathbf{a}_n \in \mathbb{R}^q$, we have $\sum_{i,j=1}^n \mathbf{a}_i^\top \mathbf{C}(\mathbf{s}_i - \mathbf{s}_j) \mathbf{a}_j \geq 0$. Genton and Kleiber (2015) provide a comprehensive review of cross-covariance functions.

While theoretical characterizations rely upon spectral theory and are useful in understanding the local behavior of random fields, perhaps the most widely used approach for constructing multivariate random fields is the linear model of coregionalization (LMC). The underlying idea is that invertible linear maps of independent spatial processes will yield valid spatial processes. If $\mathbf{f}(\mathbf{s}) = (f_1(\mathbf{s}), f_2(\mathbf{s}), \dots, f_K(\mathbf{s}))^\top$ is a $K \times 1$ vector of independent spatial processes so that $\text{cov}\{f_i(\mathbf{s}), f_j(\mathbf{s}')\} = 0$ for all $i \neq j$ and any two locations \mathbf{s} and \mathbf{s}' (same or distinct), then LMC (Bourgault and Marcotte, 1991) specifies the $q \times 1$ process

$$\mathbf{z}(\mathbf{s}) = \sum_{k=1}^K \lambda_k f_k(\mathbf{s}) = \mathbf{\Lambda}^\top \mathbf{f}(\mathbf{s}), \quad (\text{II.1})$$

where $\mathbf{\Lambda}$ is $K \times q$, λ_k^\top is the k -th row of $\mathbf{\Lambda}$ and each $f_k(\mathbf{s})$ is an independent Gaussian process with correlation function $\rho_{\psi_k}(\cdot, \cdot)$ with parameters ψ_k . The cross-covariance for $\mathbf{z}(\mathbf{s})$ yields non-degenerate process-realizations whenever $K \geq q$ and $\mathbf{\Lambda}$ is nonsingular. To achieve dimension reduction in the number of variables, we restrict $K < q$ so we have non-degenerate realizations in a K dimensional sub-space. The key question, then, is how to model $\mathbf{\Lambda}$, whose rows determine the subspace where the factors are mapped.

Other versions of LMC include Schmidt and Gelfand (2003), who model the multivariate spatial process through a hierarchical spatial conditional modeling approach, whereupon $\mathbf{\Lambda}^\top$ in (II.1) is a $q \times q$ lower triangular matrix. The flexibility offered in modeling $\mathbf{\Lambda}$ is appealing and, in particular, can accrue computational benefits in high-dimensional settings. Other approaches for building cross-covariance functions such as convolutions, latent dimensions, Matérn cross-covariances and other methods reviewed in Genton and Kleiber (2015) do not necessarily provide the flexibility and scalability we seek. Hence, we build upon (II.1).

I. A Bayesian LMC factor model

Let $\mathbf{y}(\mathbf{s}) = (y_1(\mathbf{s}), \dots, y_q(\mathbf{s}))^\top \in \mathbb{R}^q$ denote the $q \times 1$ vector of dependent outcomes in location $\mathbf{s} \in \mathcal{D} \subset \mathbb{R}^d$, $\mathbf{x}(\mathbf{s}) = (x_1(\mathbf{s}), \dots, x_p(\mathbf{s}))^\top \in \mathbb{R}^p$ be the corresponding explanatory variables, and $\boldsymbol{\beta}$ be a $p \times q$ regression coefficient matrix in the multivariate spatial model

$$\mathbf{y}(\mathbf{s}) = \boldsymbol{\beta}^\top \mathbf{x}(\mathbf{s}) + \mathbf{\Lambda}^\top \mathbf{f}(\mathbf{s}) + \boldsymbol{\epsilon}(\mathbf{s}), \quad \mathbf{s} \in \mathcal{D}, \quad (\text{II.2})$$

where the latent process $\mathbf{\Lambda}^\top \mathbf{f}(\mathbf{s})$ is an LMC as described above. Elements in $\mathbf{f}(\mathbf{s})$ are as described in (II.1), while the noise process $\boldsymbol{\epsilon}(\mathbf{s}) \stackrel{iid}{\sim} \mathbf{N}(\mathbf{0}, \boldsymbol{\Sigma})$ with covariance matrix $\boldsymbol{\Sigma}$. We model $\{\boldsymbol{\beta}, \mathbf{\Lambda}, \boldsymbol{\Sigma}\}$

using a Matrix-Normal-Inverse-Wishart family. To be precise,

$$\boldsymbol{\beta} \mid \boldsymbol{\Sigma} \sim \text{MN}(\boldsymbol{\mu}_\beta, \mathbf{V}_\beta, \boldsymbol{\Sigma}) ; \boldsymbol{\Lambda} \mid \boldsymbol{\Sigma} \sim \text{MN}(\boldsymbol{\mu}_\Lambda, \mathbf{V}_\Lambda, \boldsymbol{\Sigma}) ; \boldsymbol{\Sigma} \sim \text{IW}(\boldsymbol{\Psi}, \nu) \quad , \quad (\text{II.3})$$

where $\boldsymbol{\mu}_\Lambda$ a $q \times K$ matrix and \mathbf{V}_Λ a $K \times K$ positive definite matrix. A random matrix $\mathbf{Z}_{n \times p} \sim \text{MN}_{n,p}(\mathbf{M}, \mathbf{U}, \mathbf{V})$ has the probability density function (Dawid, 1981)

$$p(\mathbf{Z} \mid \mathbf{M}, \mathbf{U}, \mathbf{V}) = \frac{\exp\left(-\frac{1}{2} \text{tr}[\mathbf{V}^{-1}(\mathbf{Z} - \mathbf{M})^T \mathbf{U}^{-1}(\mathbf{Z} - \mathbf{M})]\right)}{(2\pi)^{np/2} |\mathbf{V}|^{n/2} |\mathbf{U}|^{p/2}} \quad , \quad (\text{II.4})$$

where $\text{tr}(\cdot)$ is the trace function, \mathbf{M} is the mean matrix, \mathbf{U} is the first scale matrix with dimension $n \times n$ and \mathbf{V} is the second scale matrix with dimension $p \times p$. This distribution is equivalent to $\text{vec}(\mathbf{Z}) \sim \text{N}_{np}(\text{vec}(\mathbf{M}), \mathbf{V} \otimes \mathbf{U})$, where \otimes is the Kronecker product and $\text{vec}(\mathbf{Z}) = [\mathbf{z}_1^\top, \dots, \mathbf{z}_p^\top]^\top$ is the vectorized $n \times p$ random matrix $\mathbf{Z} = [\mathbf{z}_1 : \dots : \mathbf{z}_p]$.

The assigned priors in (II.3) yield conditional posterior distributions in a closed form for all the parameters, except $\{\psi_k\}_{k=1}^K$. This supports a block update MCMC algorithm for posterior sampling (see Section II). If $\mathcal{S} = \{\mathbf{s}_1, \dots, \mathbf{s}_n\}$ denotes the set of locations that have recorded at least one of the observed outcomes, then $\cup_{i=1}^q \mathcal{S}_i = \mathcal{S}$, where \mathcal{S}_i is the subset of locations that have recorded the i -th response. Let $\mathcal{M}_i = \mathcal{S} \setminus \mathcal{S}_i$ denote the set of locations where at least one response, but not the i th response, is recorded so that $\cup_{i=1}^q \mathcal{M}_i = \mathcal{M}$. Without misalignment, the observation model can be cast as

$$\mathbf{Y}_{n \times q} = \mathbf{X}_{n \times p} \boldsymbol{\beta}_{p \times q} + \mathbf{F}_{n \times K} \boldsymbol{\Lambda}_{K \times q} + \boldsymbol{\epsilon}_{n \times q} \quad , \quad (\text{II.5})$$

where $\mathbf{Y} = \mathbf{y}(\mathcal{S}) = [\mathbf{y}(\mathbf{s}_1) : \dots : \mathbf{y}(\mathbf{s}_n)]^\top$ is the $n \times q$ response matrix, $\mathbf{X} = \mathbf{x}(\mathcal{S}) = [\mathbf{x}(\mathbf{s}_1) : \dots : \mathbf{x}(\mathbf{s}_n)]^\top$ is the corresponding design matrix with full rank ($n > p$), and \mathbf{F} is the $n \times K$ matrix with j -th column being the $n \times 1$ vector comprising $f_j(\mathbf{s}_i)$'s for $i = 1, 2, \dots, n$.

We derive the conditional distribution of \mathbf{F} and of the unobserved responses $\{y_i(\mathcal{M}_i)\}_{i=1}^q$ conditional on $\{\boldsymbol{\beta}, \boldsymbol{\Lambda}, \boldsymbol{\Sigma}, \{\psi_k\}_{k=1}^K\}$. Let \mathbf{P} be the permutation matrix such that $\mathbf{P} \text{vec}(\mathbf{Y}) = \{\mathbf{y}(\mathbf{s}_i)_{os_i}\}_{i=1}^n$, where the suffix os denotes the index of the observed responses for $\mathbf{s} \in \mathcal{S}$. Therefore, \mathbf{P} reorders the observed responses from $\text{vec}(\mathbf{Y})$ in locations $\{\mathbf{s}_1, \dots, \mathbf{s}_n\}$. The joint distribution of $\text{vec}(\mathbf{F})$ and $\{\mathbf{y}(\mathbf{s}_i)_{os_i}\}_{i=1}^n$, given $\{\boldsymbol{\beta}, \boldsymbol{\Lambda}, \boldsymbol{\Sigma}, \{\psi_k\}_{k=1}^K\}$, can be represented through the augmented linear system,

$$\begin{bmatrix} \{(\mathbf{y}(\mathbf{s}_i) - \mathbf{x}(\mathbf{s}_i)^\top \boldsymbol{\beta})_{os_i}\}_{i=1}^n \\ \mathbf{0} \end{bmatrix} = \begin{bmatrix} \mathbf{P}(\boldsymbol{\Lambda}^\top \otimes \mathbf{I}_n) \\ \mathbf{I}_K \otimes \mathbf{I}_n \end{bmatrix} \text{vec}(\mathbf{F}) + \begin{bmatrix} \boldsymbol{\epsilon}_1 \\ \boldsymbol{\epsilon}_2 \end{bmatrix} \quad , \quad (\text{II.6})$$

where $\boldsymbol{\epsilon}_1 \sim \text{N}(\mathbf{0}, \oplus_{i=1}^n \{\boldsymbol{\Sigma}_{os_i}\})$, $\boldsymbol{\epsilon}_2 \sim \text{N}(\mathbf{0}, \oplus_{k=1}^K \{\boldsymbol{\rho}_{\psi_k}(\mathcal{S}, \mathcal{S})\})$, $\boldsymbol{\rho}_{\psi_k}(\mathcal{S}, \mathcal{S})$ is the $n \times n$ spatial correlation matrix corresponding to $\mathbf{f}_k = (f_k(\mathbf{s}_1), f_k(\mathbf{s}_2), \dots, f_k(\mathbf{s}_n))^\top$, and $\oplus_{i=1}^n$ represents the block diagonal operator stacking matrices along the diagonal. Letting $\mathbf{D}_{\boldsymbol{\Sigma}_o}^{-\frac{1}{2}} = \oplus_{i=1}^n \{\boldsymbol{\Sigma}_{os_i}^{-\frac{1}{2}}\}$ and $\mathbf{V}_\mathbf{F} = \oplus_{k=1}^K \{\mathbf{V}_k\}$, where $\boldsymbol{\rho}_{\psi_k}^{-1}(\mathcal{S}, \mathcal{S}) = \mathbf{V}_k^\top \mathbf{V}_k$, we obtain

$$\underbrace{\begin{bmatrix} \mathbf{D}_{\boldsymbol{\Sigma}_o}^{-\frac{1}{2}} \{(\mathbf{y}(\mathbf{s}_i) - \mathbf{x}(\mathbf{s}_i)^\top \boldsymbol{\beta})_{os_i}\}_{i=1}^n \\ \mathbf{0} \end{bmatrix}}_{\tilde{\mathbf{Y}}} = \underbrace{\begin{bmatrix} \mathbf{D}_{\boldsymbol{\Sigma}_o}^{-\frac{1}{2}} \mathbf{P} \boldsymbol{\Lambda}^\top \otimes \mathbf{I}_n \\ \mathbf{V}_\mathbf{F} \end{bmatrix}}_{\tilde{\mathbf{X}}} \text{vec}(\mathbf{F}) + \underbrace{\begin{bmatrix} \boldsymbol{\eta}_1 \\ \boldsymbol{\eta}_2 \end{bmatrix}}_{\tilde{\boldsymbol{\eta}}} \quad . \quad (\text{II.7})$$

The elements of $\tilde{\boldsymbol{\eta}}$ are independent error terms, each with unit variance. The full conditional distribution $\text{vec}(\mathbf{F}) \mid \{\mathbf{y}(\mathbf{s}_i)_{os_i}\}_{i=1}^n, \boldsymbol{\beta}, \boldsymbol{\Lambda}, \boldsymbol{\Sigma}, \{\psi_k\}_{k=1}^K$ for the LMC model in (II.2) then follows

$$\text{vec}(\mathbf{F}) \mid \{\mathbf{y}(\mathbf{s}_i)_{os_i}\}_{i=1}^n, \boldsymbol{\beta}, \boldsymbol{\Lambda}, \boldsymbol{\Sigma}, \{\psi_k\}_{k=1}^K \sim \text{N}((\tilde{\mathbf{X}}^\top \tilde{\mathbf{X}})^{-1} \tilde{\mathbf{X}}^\top \tilde{\mathbf{Y}}, (\tilde{\mathbf{X}}^\top \tilde{\mathbf{X}})^{-1}). \quad (\text{II.8})$$

Turning to the unobserved variables, let ms be the suffix for $\mathbf{s} \in \mathcal{M}$. Then, the conditional distribution of $\mathbf{y}(\mathbf{s})_{ms}$ given the parameters $\{\mathbf{F}, \{\mathbf{y}(\mathbf{s}_i)_{os_i}\}_{i=1}^n, \boldsymbol{\beta}, \boldsymbol{\Lambda}, \boldsymbol{\Sigma}\}$ is

$$\mathcal{N}([\boldsymbol{\mu}_{\mathbf{s}}]_{ms} + \boldsymbol{\Sigma}_{[ms,os]} \boldsymbol{\Sigma}_{[os,os]}^{-1} (\mathbf{y}(\mathbf{s})_{os} - [\boldsymbol{\mu}_{\mathbf{s}}]_{os}), \boldsymbol{\Sigma}_{[ms,ms]} - \boldsymbol{\Sigma}_{[ms,os]} \boldsymbol{\Sigma}_{[os,os]}^{-1} \boldsymbol{\Sigma}_{[os,ms]}), \quad (\text{II.9})$$

where $\boldsymbol{\mu}_{\mathbf{s}} = \boldsymbol{\beta}^\top \mathbf{x}(\mathbf{s}) + \boldsymbol{\Lambda} \mathbf{f}(\mathbf{s})$, $\boldsymbol{\Sigma}_{[ms,os]}$ is a sub-matrix of $\boldsymbol{\Sigma}$ extracted with row index ms and column index os , and $\boldsymbol{\Sigma}_{[os,os]}^{-1}$ is the inverse of matrix $\boldsymbol{\Sigma}_{[os,os]}$. With the priors given in (II.3), we let $\mathbf{V}_\Lambda = \mathbf{L}_\Lambda \mathbf{L}_\Lambda^\top$ and define $\boldsymbol{\gamma} = [\boldsymbol{\beta}^\top, \boldsymbol{\Lambda}^\top]^\top$. The conditional posterior distribution $\boldsymbol{\gamma} \mid \boldsymbol{\Sigma}, \mathbf{F}, \mathbf{Y}$ can be found through the augmented linear system,

$$\underbrace{\begin{bmatrix} \mathbf{Y} \\ \mathbf{L}_\beta^{-1} \boldsymbol{\mu}_\beta \\ \mathbf{L}_\Lambda^{-1} \boldsymbol{\mu}_\Lambda \end{bmatrix}}_{\mathbf{Y}^*} = \underbrace{\begin{bmatrix} \mathbf{X} & \mathbf{F} \\ \mathbf{L}_\beta^{-1} & \mathbf{0} \\ \mathbf{0} & \mathbf{L}_\Lambda^{-1} \end{bmatrix}}_{\mathbf{X}^*} \underbrace{\begin{bmatrix} \boldsymbol{\beta} \\ \boldsymbol{\Lambda} \end{bmatrix}}_{\boldsymbol{\gamma}} + \underbrace{\begin{bmatrix} \eta_1 \\ \eta_2 \\ \eta_3 \end{bmatrix}}_{\boldsymbol{\eta}^*}, \quad (\text{II.10})$$

where $\boldsymbol{\eta}^* \sim \text{MN}(\mathbf{0}_{(n+p+K) \times q}, \mathbf{I}_{n+p+K}, \boldsymbol{\Sigma})$. Using standard distribution theory, we can show that $\boldsymbol{\gamma}, \boldsymbol{\Sigma} \mid \mathbf{F}, \mathbf{Y}$ follows $\text{MNIW}(\boldsymbol{\mu}^*, \mathbf{V}^*, \boldsymbol{\Psi}^*, \nu^*)$, where

$$\begin{aligned} \mathbf{V}^* &= [\mathbf{X}^{*\top} \mathbf{X}^*]^{-1}, \quad \boldsymbol{\mu}^* = \mathbf{V}^* [\mathbf{X}^{*\top} \mathbf{Y}^*], \\ \boldsymbol{\Psi}^* &= \boldsymbol{\Psi} + (\mathbf{Y}^* - \mathbf{X}^* \boldsymbol{\mu}^*)^\top (\mathbf{Y}^* - \mathbf{X}^* \boldsymbol{\mu}^*), \quad \nu^* = \nu. \end{aligned} \quad (\text{II.11})$$

In particular, if $\boldsymbol{\Sigma} = \bigoplus_{i=1}^q \{\sigma_i^2\}$, then we specify $\sigma_i^2 \sim \text{IG}(a_i, b_i)$ for $i = 1, \dots, q$ where $a_1 = a_2 = \dots = a_q = a$. We can show that the marginal posterior distribution of σ_i^2 given \mathbf{Y}, \mathbf{F} follows $\text{IG}(a^*, b_i^*)$ with

$$a^* = a + \frac{n}{2}, \quad b_i^* = b_i + \frac{1}{2} (\mathbf{Y}^* - \mathbf{X}^* \boldsymbol{\mu}^*)_i^\top (\mathbf{Y}^* - \mathbf{X}^* \boldsymbol{\mu}^*)_i, \quad i = 1, \dots, q. \quad (\text{II.12})$$

Here $(\mathbf{Y}^* - \mathbf{X}^* \boldsymbol{\mu}^*)_i$ is the i -th column of $\mathbf{Y}^* - \mathbf{X}^* \boldsymbol{\mu}^*$. Through the linear system (II.10), the conditional distribution $\boldsymbol{\gamma} \mid \boldsymbol{\Sigma}, \mathbf{F}, \mathbf{Y}$ follows $\text{MN}(\boldsymbol{\mu}^*, \mathbf{V}^*, \boldsymbol{\Sigma})$.

The full conditional distributions for $\{\psi_k\}_{k=1}^K$ are not available in closed form. However, since $\{\psi_k\}_{k=1}^K$ and \mathbf{Y} are conditionally independent given $\{\mathbf{F}, \boldsymbol{\gamma}, \boldsymbol{\Sigma}\}$, and \mathbf{f}_k are independent for $k = 1, 2, \dots, K$, we obtain $p(\psi_k \mid \mathbf{F}, \mathbf{Y}, \boldsymbol{\gamma}, \boldsymbol{\Sigma}, \{\psi_j\}_{j \neq k})$ up to a proportionality constant as

$$p(\mathbf{Y} \mid \mathbf{F}, \boldsymbol{\gamma}, \boldsymbol{\Sigma}) \times p(\boldsymbol{\gamma}, \boldsymbol{\Sigma}) \times \prod_{k=1}^K p(\mathbf{f}_k \mid \psi_k) \times p(\psi_k) \propto p(\mathbf{f}_k \mid \psi_k) \times p(\psi_k), \quad (\text{II.13})$$

for each $k = 1, \dots, K$, where $p(\psi_k)$ is the prior for ψ_k . Often, the right hand side of (II.13) is much easier to calculate than a direct formulation of the posterior distribution of ψ_k , especially when \mathbf{f}_k 's are modeled using scalable spatial models.

Turning to predictions, if $\mathcal{U} = \{\mathbf{u}_1, \dots, \mathbf{u}_{n'}\}$ is a set of new locations, then $\mathbf{Y}_{\mathcal{U}} = \mathbf{y}(\mathcal{U})$ is independent of $\{\mathbf{y}(\mathbf{s}_i)_{os_i}\}_{i=1}^n$ given $\{\boldsymbol{\beta}, \boldsymbol{\Lambda}, \boldsymbol{\Sigma}\}$ and $\mathbf{F}_{\mathcal{U}} = [\mathbf{f}_1(\mathcal{U}) : \dots : \mathbf{f}_K(\mathcal{U})]^\top$. Then,

$$\mathbf{f}_k(\mathcal{U}) \mid \mathbf{f}_k, \psi_k \sim \mathcal{N}(\boldsymbol{\rho}_{\psi_k}(\mathcal{U}, \mathcal{S}) \boldsymbol{\rho}_{\psi_k}^{-1}(\mathcal{S}, \mathcal{S}) \mathbf{f}_k, \boldsymbol{\rho}_{\psi_k}(\mathcal{U}, \mathcal{S}) \boldsymbol{\rho}_{\psi_k}^{-1}(\mathcal{S}, \mathcal{S}) \boldsymbol{\rho}_{\psi_k}(\mathcal{S}, \mathcal{U})), \quad (\text{II.14})$$

for each $k = 1, 2, \dots, K$. It follows that $p(\mathbf{Y}_{\mathcal{U}}, \mathbf{F}_{\mathcal{U}} \mid \{\mathbf{y}(\mathbf{s}_i)_{os_i}\}_{i=1}^n)$ is proportional to

$$p(\mathbf{Y}_{\mathcal{U}} \mid \mathbf{F}_{\mathcal{U}}, \boldsymbol{\beta}, \boldsymbol{\Lambda}, \boldsymbol{\Sigma}) \times p(\mathbf{F}_{\mathcal{U}} \mid \mathbf{F}, \{\psi_k\}_{k=1}^K) \times p(\boldsymbol{\beta}, \boldsymbol{\Lambda}, \boldsymbol{\Sigma}, \mathbf{F}, \{\psi_k\}_{k=1}^K \mid \{\mathbf{y}(\mathbf{s}_i)_{os_i}\}_{i=1}^n), \quad (\text{II.15})$$

where we have used the independence between $\mathbf{F}_{\mathcal{U}}$ and $\{\mathbf{y}(\mathbf{s}_i)_{os_i}\}_{i=1}^n$ given \mathbf{F} and $\{\psi_k\}_{k=1}^K$. The distributions in (II.14) and (II.15) help in sampling from the posterior predictive distribution over \mathcal{U} using the posterior samples of $\{\boldsymbol{\beta}, \boldsymbol{\Lambda}, \boldsymbol{\Sigma}, \mathbf{F}, \{\psi_k\}_{k=1}^K\}$. We elaborate below.

II. The block update MCMC algorithm

We formulate an efficient MCMC algorithm for obtaining full Bayesian inference as follows. From the l th iteration with $\{\boldsymbol{\beta}^{(l)}, \boldsymbol{\Lambda}^{(l)}, \boldsymbol{\Sigma}^{(l)}, \{\psi_k^{(l)}\}_{k=1}^K\}$, we generate $\mathbf{F}^{(l+1)}$ from (II.8). Next, we impute the missing response $\{\mathbf{y}(\mathbf{s}_i)_{mi}^{(l+1)}\}_{\mathbf{s}_i \in \mathcal{M}}$ on \mathcal{M} through (II.9) and then update $\{\boldsymbol{\beta}^{(l+1)}, \boldsymbol{\Lambda}^{(l+1)}, \boldsymbol{\Sigma}^{(l+1)}\}$ using (II.11). We complete the iteration by drawing $\{\psi_k^{(l+1)}\}_{k=1}^K$ through a Metropolis random walk using (II.13). Upon convergence, these iterations will generate samples from the desired joint posterior distribution.

For inference on \mathcal{U} , we sample $\mathbf{F}_{\mathcal{U}}$ from (II.14), given the posterior samples of \mathbf{F} and $\{\psi_k\}_{k=1}^K$, then generate posterior predictions of $\mathbf{Y}_{\mathcal{U}}$ given the posterior samples of $\{\boldsymbol{\beta}, \boldsymbol{\Lambda}, \boldsymbol{\Sigma}, \mathbf{F}_{\mathcal{U}}\}$. Applying the SCAM algorithm introduced in Haario et al. (2005), one can avoid tuning parameters in Metropolis algorithm by warming up each MCMC chain of $\{\psi_k\}_{k=1}^K$ with an adaptive proposal distribution. In our implementation, we use the proposal distribution defined by equation (2.1) in Roberts and Rosenthal (2009) with an empirical estimate of the covariance of the target distribution based on half of the chain's history. Details are provided in Sections IV and V.

The parameters $\boldsymbol{\Lambda}$ and \mathbf{F} are not jointly identified, but we can transform back to $\boldsymbol{\omega} = \mathbf{F}\boldsymbol{\Lambda}$ and obtain inference for the latent process. This parametrization has the advantage of conditional conjugacy, which brings more efficient computation in posterior sampling. We sample the elements of \mathbf{F} as a single block through a linear transformation of the $n \times K$ independent parameters from the model in (II.7). The sampling of $\{\boldsymbol{\beta}, \boldsymbol{\Lambda}\}$ follows analogously. Hence, we can significantly improve convergence by reducing the posterior dependence among the parameter in this Gibbs with Metropolis algorithm (Gelman et al., 2013). Since \mathbf{F} is sensitive to the value of the intercept, we recommend using an intercept-centered latent process to obtain inference for the latent spatial pattern and the non-spatial covariance of the latent process. We also advise against an initializing $\boldsymbol{\Lambda}$ with a zero matrix. Otherwise, \mathbf{F} may get an extreme initial value, slowing down the convergence of the MCMC chains.

III. Scalable Modeling for Block-update MCMC

We use a conjugate gradient method to facilitate the sampling of \mathbf{F} when $\boldsymbol{\rho}_{\psi_k}^{-1}(\mathcal{S}, \mathcal{S})$ is sparse for $k = 1, \dots, K$. Accelerating MCMC sampling through a conjugate gradient method has an elaborate implementation in Nishimura and Suchard (2018). We develop a Bayesian framework to implement this sampling scheme in massive multivariate spatial data modeling. Here, we illustrate a detailed algorithm for a BLMC model, where each element of the factor process $\mathbf{f}(\mathbf{s})$ is modeled as a Nearest-Neighbor Gaussian Process (NNGP).

Let each $f_k(\mathbf{s}), \mathbf{s} \in \mathcal{D}$ be an NNGP($0, \rho_{\psi_k}(\cdot, \cdot)$), which implies that $\mathbf{f}_k \sim \mathbf{N}(\mathbf{0}, \tilde{\boldsymbol{\rho}}_k)$ for each $k = 1, 2, \dots, K$, where $\tilde{\boldsymbol{\rho}}_k = (\mathbf{I} - \mathbf{A}_{\rho_k})^{-1} \mathbf{D}_{\rho_k} (\mathbf{I} - \mathbf{A}_{\rho_k})^{-\top}$, \mathbf{A}_{ρ_k} is a sparse-lower triangular matrix with no more than a specified small number, m , of nonzero entries in each row and \mathbf{D}_{ρ_k} is a diagonal matrix. The diagonal entries of \mathbf{D}_{ρ_k} and the nonzero entries of \mathbf{A}_{ρ_k} are obtained from the conditional variance and conditional expectations for a Gaussian process with covariance function $\rho_{\psi_k}(\mathbf{s}, \mathbf{s}')$. To be precise, we consider a fixed order of locations in \mathcal{S} and define $N_m(\mathbf{s}_i)$ to be the set comprising at most m neighbors of \mathbf{s}_i among locations $\mathbf{s}_j \in \mathcal{S}$ such that $j < i$. The (i, j) -th entry of \mathbf{A}_{ρ_k} is 0 whenever $\mathbf{s}_j \notin N_m(\mathbf{s}_i)$. If $j_1 < j_2 < \dots < j_m$ are the m column indices for the nonzero entries in the i -th row of \mathbf{A}_{ρ_k} , then the (i, j_k) -th element of \mathbf{A}_{ρ_k} is the k -th element of the $1 \times m$ vector $\mathbf{a}_i^\top = \boldsymbol{\rho}_{\psi_k}(\mathbf{s}_i, N_m(\mathbf{s}_i)) \boldsymbol{\rho}_{\psi_k}(N_m(\mathbf{s}_i), N_m(\mathbf{s}_i))^{-1}$. The (i, i) -th diagonal element of \mathbf{D}_{ρ_k} is given by $\rho_{\psi_k}(\mathbf{s}_i, \mathbf{s}_i) - \mathbf{a}_i^\top \boldsymbol{\rho}_{\psi_k}(N_m(\mathbf{s}_i), \mathbf{s}_i)$. Repeating these calculations for each row completes the construction of \mathbf{A}_{ρ_k} and \mathbf{D}_{ρ_k} and yields a sparse $\tilde{\boldsymbol{\rho}}_k^{-1}$. This construction can be performed in

parallel and requires storage or computation of at most $m \times m$ matrices, where $m \ll n$, costing $\mathcal{O}(n)$ flops and storage. A detailed algorithm of the MCMC algorithm for NNGP based BLMC model is presented in Appendix S.1

Sampling \mathbf{F} is computationally expensive, but is expedited by solving $(\tilde{\mathbf{X}}^\top \tilde{\mathbf{X}})^{-1} \tilde{\mathbf{X}}^\top \mathbf{v}$ efficiently for any vector \mathbf{v} . If $\rho_{\psi_k}(\mathcal{S}, \mathcal{S}) = \mathbf{L}_k \mathbf{L}_k^\top$ has a sparse Cholesky factor \mathbf{L}_k , then calculating $\tilde{\mathbf{X}}^\top \mathbf{v}$ is efficient. To be precise, the Woodbury matrix identity yields

$$(\tilde{\mathbf{X}}^\top \tilde{\mathbf{X}})^{-1} = (\mathbf{F} \mathbf{D}_{\Sigma_0}^{-1} \mathbf{F}^\top + \oplus_{k=1}^K \{\rho_k^{-1}\})^{-1} = \oplus_{k=1}^K \{\rho_k\} - \oplus_{k=1}^K \{\rho_k\} \mathbf{F} \mathbf{G}^{-1} \mathbf{F}^\top \oplus_{k=1}^K \{\rho_k\}, \quad (\text{II.16})$$

where $\mathbf{F} = \mathbf{\Lambda} \otimes \mathbf{I}_n \mathbf{P}^\top$ is sparse, $\mathbf{G} = \mathbf{D}_{\Sigma_0} + \mathbf{P} \{ \sum_{k=1}^K \lambda_{ik} \lambda_{jk} \rho_k \}_{i,j=1}^p \mathbf{P}^\top$ with $\rho_k = \rho_{\psi_k}(\mathcal{S}, \mathcal{S})$. If all the ρ_k 's have similar structures, then permuting $\{ \sum_{k=1}^K \lambda_{ik} \lambda_{jk} \rho_k \}_{i,j=1}^p$ with \mathbf{P} in rows and columns often renders sparsity in the Cholesky decomposition of ρ_k . For example, if ρ_k 's are banded matrices with bandwidth b , then $\mathbf{P} \{ \sum_{k=1}^K \lambda_{ik} \lambda_{jk} \rho_k \}_{i,j=1}^p \mathbf{P}^\top$ is also banded with bandwidth bq . Moreover, \mathbf{D}_{Σ_0} is a banded matrix with bandwidth $\leq q$. Hence, adding \mathbf{D}_{Σ_0} hardly increases the computational burden in the Cholesky decomposition of \mathbf{G} when q is small. Assembling all features of ρ_k , \mathbf{F} and \mathbf{G} , the calculation of $(\tilde{\mathbf{X}}^\top \tilde{\mathbf{X}})^{-1} \mathbf{u}$ for any $\mathbf{u} = \tilde{\mathbf{X}}^\top \mathbf{v}$ is scalable when multiplying \mathbf{u} with (II.16).

We conclude this section with a remark on the BLMC model with diagonal Σ . This specification is desirable for data sets with a massive number of responses q . Compared to BLMC, BLMC with diagonal Σ can avoid the quadratic growth of the number of parameters in Σ as q increases. When $K < q$, it becomes a factor model that can fit the latent process with a low-rank structure. We provide an example in the simulation section to illustrate an NNGP based factor BLMC with diagonal Σ .

III. ON POSTERIOR CONSISTENCY: LARGE-SAMPLE PROPERTIES OF POSTERIOR ESTIMATES

We present some theoretical results for the models constructed in the previous section. Specifically, we investigate the behavior of the posterior distribution as the sample size increases and establish its convergence to an oracle distribution. Here, for establishing the results, we will assume conjugate MNIW models with no misalignment. First, we assume that $\mathbf{y}(\mathbf{s})$ itself is modeled as a spatial process without explicitly introducing a latent process. Let

$$\mathbf{y}(\mathbf{s}) \sim \text{GP}(\boldsymbol{\beta}^\top \mathbf{x}(\mathbf{s}), \mathbf{C}(\cdot, \cdot)), \quad \mathbf{C}(\mathbf{s}, \mathbf{s}') = [\rho_\psi(\mathbf{s}, \mathbf{s}') + (\alpha^{-1} - 1) \delta_{\mathbf{s}=\mathbf{s}'}] \boldsymbol{\Sigma}, \quad (\text{III.1})$$

where $\rho_\psi(\cdot, \cdot)$ is a spatial correlation function defined through hyperparameter ψ , δ denotes Dirac's delta function, and $\alpha^{-1} \boldsymbol{\Sigma}$ is the non-spatial covariance matrix of $\mathbf{y}(\mathbf{s})$. The fixed scalar α represents the proportion of total variability allocated to the spatial process. This implies that $\mathbf{Y} | \boldsymbol{\beta}, \boldsymbol{\Sigma} \sim \text{MN}_{n,q}(\mathbf{X} \boldsymbol{\beta}, \mathcal{K}, \boldsymbol{\Sigma})$, where $\mathcal{K} = \rho_\psi(\mathcal{S}, \mathcal{S}) + (\alpha^{-1} - 1) \mathbf{I}_n$. We model $\{\boldsymbol{\beta}, \boldsymbol{\Sigma}\}$ using the conjugate MNIW prior

$$\boldsymbol{\beta} | \boldsymbol{\Sigma} \sim \text{MN}_{p,q}(\boldsymbol{\mu}_\beta, \mathbf{V}_r, \boldsymbol{\Sigma}), \quad \boldsymbol{\Sigma} \sim \text{IW}(\boldsymbol{\Psi}, \nu), \quad (\text{III.2})$$

with prefixed $\{\boldsymbol{\mu}_\beta, \mathbf{V}_r, \boldsymbol{\Psi}, \nu\}$. Closely following the developments in Gamerman and Moreira (2004), we obtain the posterior distribution of $\{\boldsymbol{\beta}, \boldsymbol{\Sigma}\}$ as MNIW($\boldsymbol{\mu}^*, \mathbf{V}^*, \boldsymbol{\Psi}^*, \nu^*$), where

$$\begin{aligned} \mathbf{V}^* &= (\mathbf{X}^\top \mathcal{K}^{-1} \mathbf{X} + \mathbf{V}_r^{-1})^{-1}, \quad \boldsymbol{\mu}^* = \mathbf{V}^* (\mathbf{X}^\top \mathcal{K}^{-1} \mathbf{Y} + \mathbf{V}_r^{-1} \boldsymbol{\mu}_\beta), \\ \boldsymbol{\Psi}^* &= \boldsymbol{\Psi} + \mathbf{Y}^\top \mathcal{K}^{-1} \mathbf{Y} + \boldsymbol{\mu}_\beta^\top \mathbf{V}_r^{-1} \boldsymbol{\mu}_\beta - \boldsymbol{\mu}^{*\top} \mathbf{V}^{*-1} \boldsymbol{\mu}^*, \quad \text{and } \nu^* = \nu + n. \end{aligned} \quad (\text{III.3})$$

We refer to the above model as the ‘‘response’’ model.

Next, we consider the spatial regression model with the latent process,

$$\mathbf{y}(\mathbf{s}) = \boldsymbol{\beta}^\top \mathbf{x}(\mathbf{s}) + \boldsymbol{\omega}(\mathbf{s}) + \boldsymbol{\epsilon}(\mathbf{s}), \quad \mathbf{s} \in \mathcal{D}, \quad (\text{III.4})$$

where $\boldsymbol{\omega}(\mathbf{s}) \sim \text{GP}(\mathbf{0}_{q \times 1}, \rho_\psi(\cdot, \cdot) \boldsymbol{\Sigma})$ is a latent process and $\boldsymbol{\epsilon}(\mathbf{s}) \sim \text{N}(\mathbf{0}_{q \times 1}, (\alpha^{-1} - 1) \boldsymbol{\Sigma})$ is measurement error. Define $\boldsymbol{\omega} = \boldsymbol{\omega}(\mathcal{S}) = [\boldsymbol{\omega}(\mathbf{s}_1) : \dots : \boldsymbol{\omega}(\mathbf{s}_n)]^\top$. For theoretical tractability, we restrict posterior inference on $\{\boldsymbol{\beta}, \boldsymbol{\omega}, \boldsymbol{\Sigma}\}$, assuming that the scalar α is fixed. Assuming that the joint distribution of $\boldsymbol{\beta}$ and $\boldsymbol{\Sigma}$ are given in (II.3) and that $\boldsymbol{\omega} \mid \boldsymbol{\Sigma} \sim \text{MN}_{n \times q}(\mathbf{0}, \rho_\psi(\mathcal{S}, \mathcal{S}), \boldsymbol{\Sigma})$, the posterior distribution of $\boldsymbol{\gamma}^\top = [\boldsymbol{\beta}^\top, \boldsymbol{\omega}^\top]$ is $p(\boldsymbol{\gamma}, \boldsymbol{\Sigma} \mid \mathbf{Y}) = \text{MNIW}(\boldsymbol{\mu}_\gamma^*, \mathbf{V}^*, \boldsymbol{\Psi}^*, \nu^*)$, where

$$\begin{aligned} \mathbf{V}^* &= \left[\begin{array}{cc} \frac{\alpha}{1-\alpha} \mathbf{X}^\top \mathbf{X} + \mathbf{V}_r^{-1} & \frac{\alpha}{1-\alpha} \mathbf{X}^\top \\ \frac{\alpha}{1-\alpha} \mathbf{X} & \rho_\psi^{-1}(\mathcal{S}, \mathcal{S}) + \frac{\alpha}{1-\alpha} \mathbf{I}_n \end{array} \right]^{-1}, \quad \boldsymbol{\mu}_\gamma^* = \mathbf{V}^* \begin{bmatrix} \frac{\alpha}{1-\alpha} \mathbf{X}^\top \mathbf{Y} + \mathbf{V}_r^{-1} \boldsymbol{\mu}_\beta \\ \frac{\alpha}{1-\alpha} \mathbf{Y} \end{bmatrix}, \\ \boldsymbol{\Psi}^* &= \boldsymbol{\Psi} + \frac{\alpha}{1-\alpha} \mathbf{Y}^\top \mathbf{Y} + \boldsymbol{\mu}_\beta^\top \mathbf{V}_r^{-1} \boldsymbol{\mu}_\beta - \boldsymbol{\mu}_\gamma^{*\top} \mathbf{V}^{*-1} \boldsymbol{\mu}_\gamma^* \quad \text{and} \quad \nu^* = \nu + n, \end{aligned} \quad (\text{III.5})$$

We refer to the above model as the ‘‘latent’’ model.

We establish the posterior consistency of $\{\boldsymbol{\beta}, \boldsymbol{\Sigma}\}$ for the response model (III.1) and the latent model (III.4). For distinguishing the variables based on the number of observations, we make the dependence upon n explicit. Denote $\mathbf{X}(n)_{n \times p} = [\mathbf{x}(\mathbf{s}_1) : \dots : \mathbf{x}(\mathbf{s}_n)]^\top$, $\mathbf{Y}(n)_{n \times q} = [\mathbf{y}(\mathbf{s}_1) : \dots : \mathbf{y}(\mathbf{s}_n)]^\top$, $\mathcal{S}(n) = \{\mathbf{s}_1, \dots, \mathbf{s}_n\}$, $\mathcal{K}(n) = \mathbf{C}(\mathcal{S}(n), \mathcal{S}(n)) + (\alpha^{-1} - 1) \mathbf{I}_n$. In the following results, we denote $\mathbf{P}(n) = \mathbf{X}(n)^\top \mathcal{K}(n)^{-1} \mathbf{X}(n)$, $\mathbf{A} \geq \mathbf{B}$ to mean that $\mathbf{A} - \mathbf{B}$ is a positive semi-definite matrix, and \mathbf{A}_{ij} to be the (i, j) -th element of \mathbf{A} . Proofs and technical details are available in Appendix S.2.

Theorem III.1. [Theorem S.2, Theorem S.3] *Parameter set $\{\boldsymbol{\beta}, \boldsymbol{\Sigma}\}$ is posterior consistent for both conjugate response and latent models if and only if $\lim_{n \rightarrow \infty} \lambda_{\min}(\mathbf{P}(n)) = \infty$, where $\lambda_{\min}(\mathbf{P}(n))$ is the smallest eigenvalue of $\mathbf{P}(n)$.*

When the explanatory variables share the same spatial correlation with the responses, the necessary and sufficient conditions for Theorem III.1 hold (see Remark S.5). When the explanatory variables are themselves regarded as independent observations, the necessary and sufficient conditions in Theorem III.1 hold (see Remark S.6).

IV. SIMULATION

We present two simulation examples here. The first compares our proposed BLMC model with other multivariate Bayesian spatial models. The second assesses our factor BLMC model when K is not excessively large. Our proposed models were implemented in Julia 1.2.0 (Bezanson et al., 2017). We modeled the univariate processes in the proposed BLMC by NNGP. We took the Bayesian LMC model proposed by Schmidt and Gelfand (2003) as a benchmark in the first simulation example. The benchmark model was implemented in R 3.4.4 through function *spMisalignLM* in the R package *spBayes* (Finley et al., 2007). We also fitted a response NNGP model with misalignment in Julia 1.2.0 in the first example. The detailed algorithms for the response NNGP model with misalignment is in Appendix S.3. The most demanding model took approximately 21 hours to deliver its entire inferential output involving 20,000 MCMC iterations on a single 8 Intel Core i7-7700K CPU @ 4.20GHz processor with 32 Gbytes of random-access memory running Ubuntu 18.04.2 LTS. Convergence diagnostics and other posterior summaries were implemented within the Julia statistical environment. Each model was compared in terms of the posterior inference of parameters (posterior mean and 95% confidence interval), root mean squared prediction error (RMSPE), mean squared error of intercept-centered latent processes (MSEL), prediction

interval coverage (CVG; the percent of intervals containing the true value), interval coverage for intercept-centered latent process of observed response (CVGL), average continuous rank probability score (CRPS; see Gneiting and Raftery (2007)) for responses, and the average interval score (INT; see Gneiting and Raftery (2007)) for responses and run time. To calculate the CRPS and INT, we assumed that the associated predictive distribution was well approximated by a Gaussian distribution with mean centered at the predicted value and standard deviation equal to the predictive standard error. All NNGP models were specified with at most $m = 10$ nearest neighbors.

I. Simulation Example 1

We simulated the response $y(\mathbf{s})$ from the LMC model in (II.2) with $q = 2, p = 2, K = 2$ over 1200 randomly generated locations over a unit square. The size of the data set was kept moderate to enable comparisons with the expensive full GP based LMC models for experiments conducted on the computing setup described earlier. The explanatory variable $\mathbf{x}(\mathbf{s})$ consists of an intercept and a single predictor generated from a standard normal distribution. An exponential correlation function was used to model $\{\rho_{\psi_k}(\cdot, \cdot)\}_{k=1}^K$, i.e., $\rho_{\psi_k}(\mathbf{s}, \mathbf{s}') = \exp(-\phi_k \|\mathbf{s} - \mathbf{s}'\|)$, for $\mathbf{s}, \mathbf{s}' \in \mathcal{D}$, where $\|\mathbf{s} - \mathbf{s}'\|$ is the Euclidean distance between \mathbf{s} and \mathbf{s}' , and $\psi_k = \phi_k$ is the decay for each k . We took $\Sigma = \text{diag}([0.3, 0.2])$ and let Λ in (II.2) be an upper triangular matrix. We randomly picked 200 locations for predicting each response to examine the predictive performance. Since the data set has misalignment, we present inference from a response NNGP model with misalignment (resp NNGP), BLMC, and the Benchmark LMC model. Table 1 presents the posterior estimates of all model parameters including the covariance matrix of the measurement error (labeled as $\text{cov}(\epsilon)$) and the non-spatial covariance of latent process (labeled as $\text{cov}(\omega)$).

We assigned flat priors for $\{\beta, \Lambda\}$ for the response NNGP model with misalignment and the BLMC. The prior for Σ for the two models was set to follow $\text{IW}(\Psi, \nu)$ with $\Psi = \text{diag}([1.0, 1.0])$ and $\nu = 3$. For the benchmark LMC, we assigned a flat prior for β , $\text{IW}(\Psi, \nu)$ with $\Psi = \text{diag}([1.0, 1.0])$ and $\nu = 3$ for the cross-covariance matrix $\Lambda^\top \Lambda$, and $\text{IG}(2, 0.5)$ for each diagonal element of Σ . The candidate values for $\{\phi, \alpha\}$ were estimated using a cross-validation algorithm for the response NNGP model (with misalignment) over a 25 by 25 grid over $[2.12, 26.52] \times [0.8, 0.99]$. We assigned $\text{unif}(2.12, 212)$ as priors of decays for BLMC and benchmark LMC model. The posterior inference from the response NNGP with misalignment, BLMC as well as the benchmark LMC model were based on an MCMC chain with 20,000 iterations, and we took the first 15,000 samples as burn-in. The number of iterations of all MCMC chains was taken to be large enough to ensure convergence.

All three models provided similar posterior inferences for $\{\beta_{21}, \beta_{21}\}$. The 95% confidence intervals of the intercepts $\{\beta_{11}, \beta_{12}\}$ all include the true value used to generate the data. With a mismatch of data generating schemes and model assumptions, the response NNGP model with misalignment provided incorrect inference for $\text{cov}(\epsilon)$ when compared to the other two candidate models. The RMSPEs and CVGs, however, are close to BLMC and benchmark LMC. Compared to benchmark LMC which cost around 21 hours, the response NNGP model spent less than 0.5 minute, suggesting that fitting the response NNGP model with misalignment is a pragmatic way to have reliable interpolation and predictions. The NNGP based BLMC model costs 4.5 minutes, while the Benchmark LMC model costs around 21 hours. Yet, despite the shorter running time, we observed superior performance of the NNGP based BLMC models than the benchmark LMC for inferring on the latent process using CVGL. Moreover, the interpolated map of the recovered intercept-centered latent processes (figure 1) by BLMC and benchmark LMC are almost indistinguishable from each other. BLMC and benchmark LMC produce very similar MSELs, RMSPEs, CRPS and INT. Benchmark LMC yields better estimates for the spatial decays but poorer

inference for $\text{cov}(\omega)$. The differences in estimates between the two models is likely emerging from the different prior settings and sampling schemes. Benchmark LMC restricts the loading matrix Λ to be upper triangular, while BLMC does not, resulting in greater flexibility in fitting latent process. On the other hand, the unidentifiable parameter setting of BLMC may cause less somewhat less stable inference for the hyperparameters $\{\phi_1, \phi_2\}$.

Table 1: Simulation study summary table: posterior mean (2.5%, 97.5%) percentiles

	True	resp NNGP	BLMC	benchmark LMC
β_{11}	1.0	0.761(0.13, 1.376)	0.877(0.399, 1.378)	0.79 (0.344, 1.229)
β_{12}	-1.0	-1.048(-1.971, -0.09)	-1.605(-2.078, -0.977)	-0.795(-2.069, 0.74)
β_{21}	-5.0	-4.958(-5.068, -4.847)	-4.968(-5.113, -4.819)	-4.968(-5.115, -4.822)
β_{22}	2.0	1.925(1.763, 2.087)	1.93(1.719, 2.124)	1.933 (1.731, 2.134)
$\text{cov}(\epsilon)_{11}$	0.3	0.17 (0.156, 0.185)	0.277 (0.231, 0.324)	0.275 (0.233, 0.326)
$\text{cov}(\epsilon)_{12}$	0.0	-0.052(-0.071, -0.036)	0.023 (-0.031, 0.073)	0.0
$\text{cov}(\epsilon)_{22}$	0.2	0.376(0.344, 0.411)	0.221 (0.145, 0.307)	0.244 (0.165, 0.322)
$\text{cov}(\omega)_{11}$	0.683	1.58(1.451, 1.719)	0.707 (0.636, 0.778)	0.706 (0.639, 0.773)
$\text{cov}(\omega)_{12}$	-0.616	-0.488 (-0.656, -0.33)	-0.596(-0.685, -0.504)	-0.07(-0.115, -0.024)
$\text{cov}(\omega)_{22}$	4.517	3.5(3.203, 3.826)	4.372 (4.2, 4.536)	4.311(4.15, 4.455)
ϕ_1	6.0	7.204($\alpha = 0.903$)	2.926(2.213, 3.941)	8.63 (5.251, 12.711)
ϕ_2	6.0	7.204($\alpha = 0.903$)	7.771(3.963, 12.226)	6.045(3.731, 8.526)
RMSPE ^a	–	[0.643, 0.948, 0.81]	[0.633, 0.917, 0.788]	[0.633, 0.918, 0.788]
MSEL ^b	–	–	[0.111, 0.139, 0.125]	[0.111, 0.14, 0.126]
CRPS ^a	–	[-0.366, -0.535, -0.45]	[-0.359, -0.515, -0.437]	[-0.359, -0.515, -0.437]
CRPSL ^b	–	–	[-0.031, -0.036, -0.033]	[-0.189, -0.212, -0.2]
CVG ^a	–	[0.945, 0.955, 0.95]	[0.965, 0.945, 0.955]	[0.965, 0.945, 0.955]
CVGL ^b	–	–	[0.941, 0.971, 0.956]	[0.791, 0.816, 0.803]
INT ^a	–	[3.031, 4.324, 3.678]	[2.929, 4.327, 3.628]	[2.927, 4.315, 3.621]
INTL ^b	–	–	[0.253, 0.278, 0.265]	[1.535, 1.728, 1.631]
time(s)	–	[14, 2, 12] ^c	270	[51456, 23973] ^d

^a[response 1, response 2, all responses]

^bintercept + latent process on 1000 observed locations for [response 1, response 2, all responses]

^c[time for cross-validation, time for MCMC sampling, time for recovering β and predictions]

^d[time for MCMC sampling, time for recovering predictions]

II. Simulation Example 2

We generated the second dataset by LMC model (II.2) with a diagonal Σ and $q = 10, p = 3, K = 50$ over 1200 randomly generated locations over a unit square. The explanatory variable $\mathbf{x}(\mathbf{s})$ was composed of an intercept and two predictors generated independently from a standard normal distribution. We used an exponential covariance function to model $\{\rho_{\psi_k}(\cdot, \cdot)\}_{k=1}^K$, where $\psi_k = \phi_k$ denotes the decay for $k = 1, \dots, K$. This data set features a relatively large number of responses ($q = 10$) and a complicated pattern in latent processes ($K = 50$). We randomly selected 200 locations for prediction for each response.

We fitted a factor BLMC model with diagonal Σ with K from 1 to 10. The goal of this simulation example is to check the performance of a factor BLMC model, especially in recovering latent processes, when K is not sufficiently large. We assigned a $\Gamma(2, 11.67)$ prior for all $\{\phi_k\}_{k=1}^K$ and

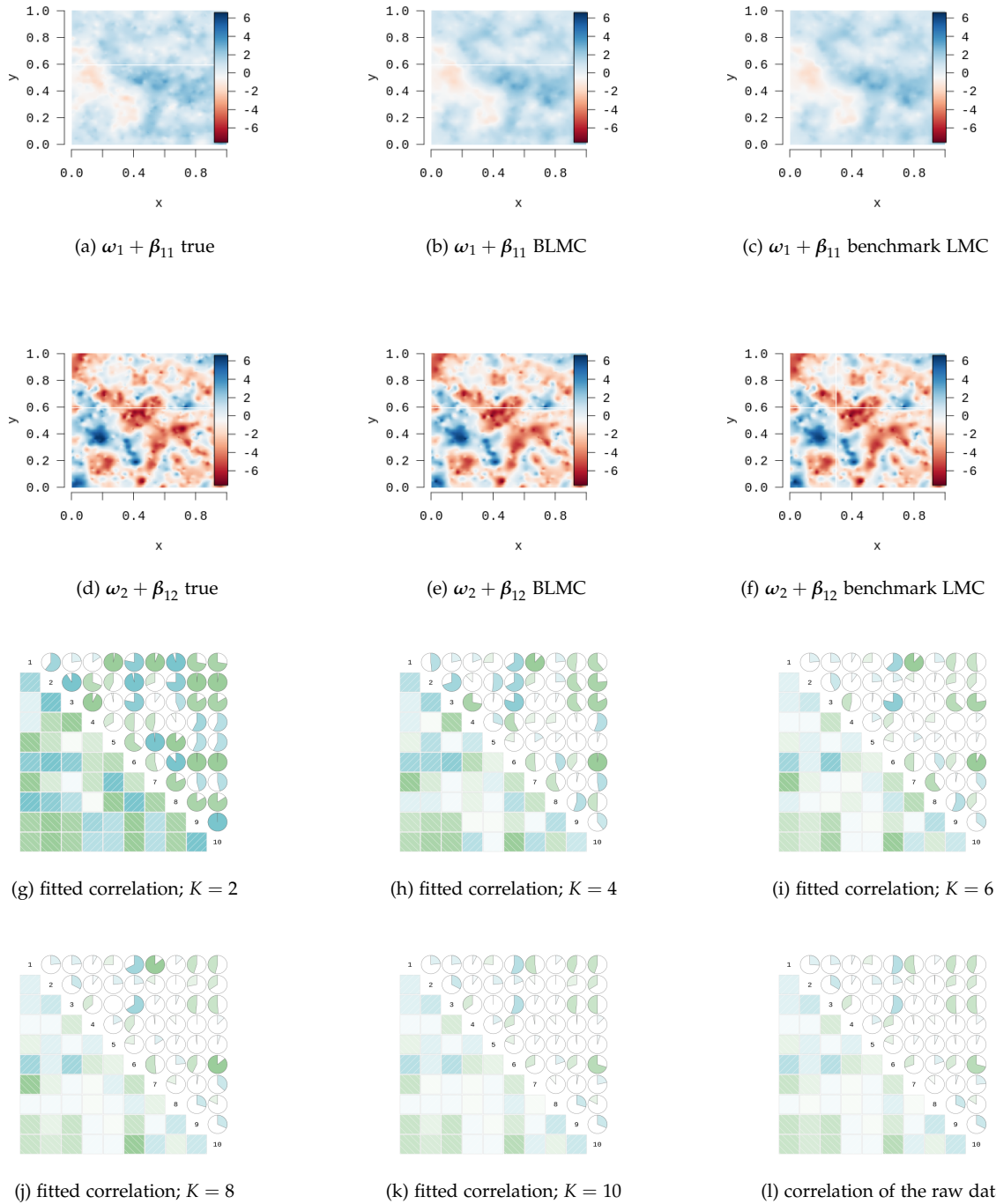


Figure 1: Interpolated maps of (a) & (d) the true generated intercept-centered latent processes, the posterior means of the intercept-centered latent process ω from the (b) & (e) NNGP based BLMC model and the (c) & (f) benchmark LMC model. Heat-maps of the (l) actual and (g)-(k) fitted non-spatial correlation of $\omega(\mathbf{s})$

Table 2: Simulation study summary table 2:

K =	1	2	3	4	5	6	7	8	9	10
CVG-slope	19/20	18/20	18/20	18/20	19/20	19/20	19/20	20/20	20/20	20/20
CVGL	0.3068	0.4175	0.5103	0.5999	0.6642	0.7236	0.7864	0.7934	0.8462	0.8681
CVG	0.9445	0.942	0.9375	0.943	0.9435	0.9435	0.941	0.938	0.9385	0.94
RMSPE	4.6531	4.3852	4.0105	3.7076	3.5578	3.2946	3.0944	2.9314	2.716	2.527
time(s)	235	422	836	1268	1891	2417	3214	3635	4880	5248

we set flat priors for β and Λ . All diagonal elements of Σ were assigned an $IG(2, 1.0)$ prior. The setting for the MCMC sampling scheme follows that of BLMC in the first example.

The running time for executing the models along with CVGL, CVG, and RMSPE are listed in table 2. We also added CVG-slope in table 2, which counts the number of 95% CIs of regression slopes that include the true value. Inference for the regression slopes was found to be robust to the choice of K . The CVG for each K was close to 0.95, while RMSPE decreased rapidly as K increased. We also found that factor BLMC would fit the latent processes better for some of the responses than the others when K was small. The performance metrics quickly improved as K increased from 1 to 10: RMSPE decreased by 45.7% while CVGL increased from 30% to over 75% for $K \geq 7$.

We compare the correlation across different latent processes (referred as non-spatial correlation) to check the performance of different models in estimating the latent processes. Figures 1g through 1l illustrate the heat-maps of the non-spatial correlation of the fitted and the true latent processes. As K increases from 2 to 10, the estimated heat-maps approach the true correlation matrix. It can be seen that the heat-map for the fitted correlation with $K = 10$ shared a similar pattern with that of the actual correlation. Given that our data comes from an LMC model with $K = 50$, we can conclude that the factor BLMC is efficient in obtaining inference for the latent processes even when K is not adequately large. The test also shows that the choice of K is important for obtaining reliable inference when using BLMC with a diagonal Σ as a factor model. We recommend choosing K based on scientific considerations for the problem at hand and exploratory data analyses. One can also check the RMSPE value for different K and use an elbow rule (Thorndike, 1953) to choose K .

V. REMOTE-SENSED VEGETATION DATA ANALYSIS

We apply our proposed models to analyze Normalized Difference Vegetation Indices (NDVI) and Enhanced Vegetation Indices (EVI) measuring vegetation activity on the land surface, which can help us understand the global distribution of vegetation types as well as their biophysical and structural properties and spatial variations. Apart from vegetation indices, we consider Gross Primary Productivity data, Global Terrestrial Evapotranspiration (ET) Product, and landcover data (see Ramon Solano et al., 2010; Mu et al., 2013; Sulla-Menashe and Friedl, 2018, for further details). The geographic coordinates of our variables were mapped on a Sinusoidal (SIN) projection grid. We chose zone *h08v05*, which covers 11,119,505 to 10,007,555 meters south of the prime meridian and 3,335,852 to 4,447,802 meters north of the equator. The land region in zone *h08v05* is situated in the western United States. Our explanatory variables included an intercept and a binary indicator for no vegetation or urban area through the 2016 landcover data. All other variables were measured through MODIS satellite over a 16-days period from 2016.04.06 to 2016.04.21. Some variables were rescaled and transformed in exploratory data analysis for the sake of better model fitting. The data sets were downloaded using the R package *MODIS* and the code for the exploratory data analysis is provided as supplementary material to this paper.

Our data set comprises 1,020,000 randomly selected observed locations to illustrate BLMC, response NNGP with misalignment and a factor BLMC model with diagonal Σ . Our spatially dependent outcomes were the transformed NDVI ($\log(\text{NDVI} + 1)$) labeled as NDVI and red reflectance (red refl). A Bayesian linear model were also fitted for comparison. All NNGP based models specified at most $m = 10$ nearest neighbors. We randomly held 10% of each response and then held all responses over region 10,400,000 to 10,300,000 meters south of the prime meridian and 3,800,000 to 3,900,000 meters north of the equator to examine the predictive performance of models over a missing region and randomly missing locations. Figure 2a illustrates the map of the transformed NDVI data. The white square region within the Continent is the region held out for prediction.

The posterior inference for BLMC and response NNGP with misalignment were based on an MCMC chain with 10,000 iterations. The priors for all parameters except decays follow those in the simulation section. We assigned $\Gamma(200, 0.02)$ and $\Gamma(200, 0.04)$ for ϕ_1 and ϕ_2 for BLMC based on variograms fitted in exploratory data analysis. We recursively shrink the domain and the grid of candidate values $\{\phi, \alpha\}$ through repeatedly using cross-validation algorithms for fixing parameters for the response NNGP model with misalignment. The number of threads used in the cross-validation algorithms for response NNGP models with misalignment were equal to the number of folders. The remaining part of all the code were run with single thread.

Table 3 gives the results of BLMC and response NNGP with misalignment. Consistent with the related background, the regression coefficients of the index of no vegetation or urban area show relatively low biomass (low NDVI) and high red reflectance over no vegetation or urban area. The inference of the covariance of the noise and non-spatial covariance of the latent process shows a negative association between the residuals and latent processes of transformed NDVI and red reflectance, which satisfies the underlying relationship between two responses. BLMC captured a high negative correlation (≈ -0.87) between the latent processes of two responses, indicating that the spatial pattern of the latent processes of NDVI and red-reflectance are almost the reverse of each other. The maps of the latent processes recovered by BLMC, presented in Figure 2, also support this relationship.

Each model was compared in terms of RMSPE, CVG, CRPS, INT and run time. It is clear that the spatial models greatly improved predictive accuracy. BLMC and the response NNGP with misalignment reduced at least 50% RMSPE compared to the Bayesian linear model. CVG is similar among all models, while all spatial models provided a more accurate prediction than the Bayesian linear models based on INT and CRPS. Visual inspections of the recovered latent processes based on BLMC are shown in figure 2. Notably, the proposed methods smooth out the predictions in the held-out region. The BLMC model took around 44.7 hours. Regarding the scale of the multivariate spatial data set, the run time for BLMC model is still appealing.

We also fitted a factor BLMC with diagonal Σ to explore the underlying latent processes of ten (transformed) responses: (i) NDVI, (ii) EVI, (iii) Gross Primary Productivity (GPP), (iv) Net Photosynthesis (PsnNet), (v) red reflectance (red refl), (vi) blue reflectance (blue refl), (vii) average daily global evapotranspiration (ET), (viii) latent heat flux (LE), (ix) potential ET (PET) and (x) potential LE (PLE). We held all responses over the region in the previous example and randomly held 10% of each response to examine the predictive performance. There are, in total, 12,057 locations with no responses and 656,366 observed locations with misaligned data (at least one but not all responses), which covers 65.12% of observed locations. We provide a heat-map (Figure 2i) to present the status of misalignment over the study domain.

Based on the exploratory analysis, we observed two groups of responses that have high within-group correlations but relatively low between-group correlations (see Figure 2g). Hence we picked $K = 2$ for the factor BLMC with diagonal Σ . The fitted results of the factor BLMC

model is presented in Table 4. No vegetation or urban area exhibits lower vegetation indexes (lower NDVI and EVI) and lower production of chemical energy in organic compounds by living organisms (lower GPP and PsnNet). We observe a trend of higher blue reflectance, red reflectance, evapotranspiration (higher ET LE) and lower potential evapotranspiration (lower PET PLE) in urban area and area with no vegetation. We provide maps of posterior predictions for all 10 variables in Appendix S.4.

The latent processes corresponding to transformed NDVI and red reflectance fitted through BLMC and the factor BLMC with diagonal Σ in Figure 2 share a similar pattern. Finally, the heat map of the nonspatial correlation of the latent processes fitted by the factor BLMC with diagonal Σ , presented in figure 2h, reveals a high underlying correlation among NDVI, EVI, GPP, PsnNet, red and blue reflectance, and that LE and ET are slightly more correlated with NDVI and EVI than PLE and PET. The total run time for factor BLMC with diagonal Σ was around 75 hours (4518.67 minutes).

Table 3: Real data analysis summary table 1: posterior mean (2.5%, 97.5%) percentiles

	Bayesian linear model	Response NNGP with misalign	BLMC
intercept ₁	0.25146(0.25117, 0.25176)	0.1662(0.1579, 0.1742)	-
intercept ₂	0.13951(0.13937, 0.13965)	0.178(0.1733, 0.1827)	-
no vege or urban area ₁	-0.1338(-0.1349, -0.1327)	-1.066e-2 (-1.085e-2, -1.047e-2)	-1.385e-2 (-1.430e-2, -1.342e-2)
no vege or urban area ₂	6.039e-2 (5.989e-2, 6.09e-2)	5.4625e-3 (5.3478e-3, 5.5733e-3)	7.831e-3 (7.584e-3, 8.097e-3)
cov(ϵ) ₁₁	1.599e-2 (1.595e-2, 1.604e-2)	2.4628e-4 (2.4566e-4, 2.4702e-4)	3.51e-4 (3.48e-4, 3.55e-4)
cov(ϵ) ₁₂	-6.494e-3(-6.515e-3, -6.474e-3)	-8.617e-5 (-8.649e-5, -8.585e-5)	-1.08e-4 (-1.10e-4, -1.07e-4)
cov(ϵ) ₂₂	3.657e-3(3.647e-3, 3.668e-3)	7.672e-5 (7.652e-5, 7.692e-5)	1.07e-4 (1.06e-4, 1.08e-4)
cov(ω) ₁₁	-	3.334e-2(3.325e-2, 3.344e-2)	1.675e-2(1.674e-2, 1.676e-2)
cov(ω) ₁₂	-	-1.166e-2(-1.171e-2, -1.162e-2)	-6.873e-3(-6.879e-3, -6.867e-3)
cov(ω) ₂₂	-	1.039e-2 (1.036e-2, 1.041e-2)	3.764e-3 (3.760e-3, 3.768e-3)
ϕ_1	-	26.414 ($\alpha = 0.99267$)	3.942 (3.857, 4.013)
ϕ_2	-	26.414($\alpha = 0.99267$)	12.358 (11.601, 13.162)
RMSPE ^a	[0.074, 0.0359, 0.0582]	[0.03172, 0.01743, 0.02559]	[0.0326, 0.0171, 0.0260]
CRPS ^a	[-0.0414, -0.01052, -0.02596]	[-0.01523, -0.00875, -0.01199]	[-0.01561, -0.00879, -0.0122]
CVG ^a	[0.9526, 0.9547, 0.9537]	[0.9515, 0.9427, 0.9471]	[0.954, 0.947, 0.950]
INT ^a	[0.34868, 0.17283, 0.26077]	[0.1909, 0.10172, 0.14631]	[0.1965, 0.09952, 0.14802]
time(mins)	-	[169.19, 65.52, 51.13] ^b	2684.75

^a[1st response transformed NDVI, 2nd response red reflectance, all responses]

^b[time for cross-validation, time for MCMC sampling, time for recovering β and predictions]

Table 4: Real data analysis summary table 2: posterior mean (2.5%, 97.5%)

response	intercept	slope	nugget (Σ_{ii})
NDVI	-0.176(-0.179, -0.172)	-0.0121 (-0.0125, -0.0116)	7.45e-4 (7.43e-4, 7.48e-4)
EVI	-0.076(-0.077, -0.074)	-4.4e-3(-4.7e-3, -4.1e-3)	8.68e-4(8.65e-4, 8.7e-4)
GPP	-6.939(-6.957, -6.919)	-0.197(-0.199, -0.194)	0.0244(0.0243, 0.0245)
PsnNet	-4.282 (-4.289, -4.275)	-4.5e-3(-5.5e-3, -3.6e-3)	5.34e-3(5.32e-3, 5.36e-3)
red refl	0.358 (0.356, 0.359)	4.5e-3 (4.2e-3, 4.8e-3)	9.84e-4(9.81e-4, 9.87e-4)
blue refl	0.186(0.185, 0.187)	0.0123 (0.0121, 0.0124)	2e-4(2.59e-4, 2.61e-4)
LE	4.601(4.586, 4.616)	0.091(0.088, 0.093)	0.0531 (0.0529, 0.0533)
ET	1.154(1.139, 1.169)	0.092 (0.089, 0.094)	0.0531(0.053, 0.0533)
PLE	0.7126 (0.7118, 0.7132)	-3.6e-3 (-3.8e-3, -3.3e-3)	2.1e-5 (2.09e-5, 2.11e-5)
PET	2.255 (2.252, 2.257)	-4.6e-3(-5.5e-3, -3.8e-3)	6.4e-5 (6.3e-5, 6.4e-5)

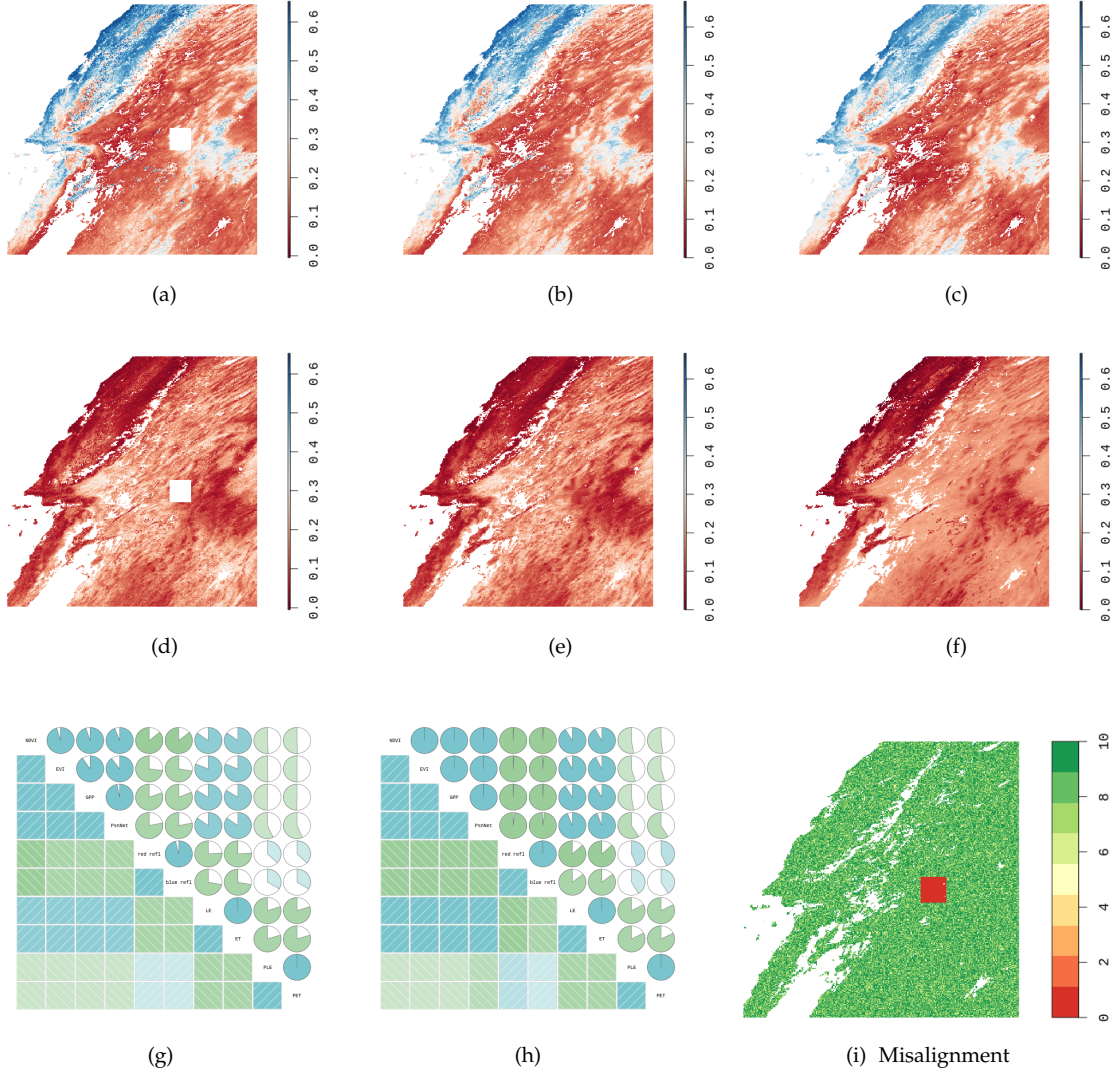


Figure 2: Colored NDVI and red reflectance images of western United States (zone h08v05). Maps of raw data (a) & (d) and the posterior mean of the intercept-centered latent process recovered from (b) & (e) BLMC and (c) & (f) factor BSLMC with diagonal Σ . Correlation of responses (g) and nonspatial correlation of latent process fitted by the factor BLMC model with diagonal Σ (h). Heat-map (k) of counts of observed response, the greener the color, the higher the count.

VI. SUMMARY AND DISCUSSION

We have proposed scalable models for analyzing massive and possibly misaligned multivariate spatial data sets. Our framework offers flexible covariance structures and scalability by modeling the loading matrix of spatial factors using Matrix-Normal distributions and the factors themselves as NNGPs. This process-based formulation allows us to resolve spatial misalignment by fully model-based imputation. Through a set of simulation examples and an analysis of a massive misaligned data set comprising remote-sensed variables, we demonstrated the inferential and

computational benefits accrued from our proposed framework.

This work can be expanded further in at least two important directions. The first is to extend the current methods to spatiotemporal data sets, where multiple variables are indexed by spatial coordinates, as considered here, as well as by temporal indices. Associations are likely to be exhibited across space and time as well as among the variables within a location and time-point. In addition, these variables are likely to be misaligned across time and space. Regarding the scalability of the spatiotemporal process, we can build a dynamic nearest-neighbor Gaussian process (DNNGP) (Datta et al., 2016b) to model spatiotemporal factors and one can also envisage temporal dependence on the loading matrix.

A second direction will consider spatially-varying coefficient models. We model the regression coefficients β using a spatial (or spatiotemporal) random field to capture spatial (or spatiotemporal) patterns in how some of the predictors impact the outcome. We can assign the prior of the regression coefficients β using a multivariate Gaussian random field with a proportional cross-covariance function. Then the prior of β over observed locations follows a Matrix-Normal distribution, which is the prior we designed for β in all of the proposed models in this article. While the modification seems to be easy, the actual implementation requires a more detailed exploration, and we leave these topics for further explorations.

From a computational perspective, we clearly need to further explore high-performance computing and high-dimensional spatial models amenable to such platforms. The programs provided in this work are for illustration and have limited usage in Graphical Processing Units (GPU) computing and parallelized CPU computing. A parallel CPU computing algorithm for the BLMC model can simultaneously sample multiple MCMC chains, improving the performance of the actual implementations. Implementations with modeling methods such as MRA (Katzfuss, 2017) also requires dedicated programming with GPU. Other scalable modeling methods that build graphical Gaussian models on space, time and the number of variables can lead to sparse models for high-dimensional multivariate data and scale not only up to millions of locations and time points, but also to hundreds or even thousands of spatially or spatiotemporally oriented variables. The idea here will be to extend current developments in Vecchia-type models to graphs building dependence among a large number of variables so that the precision matrices across space, time and variables is sparse. Research on scalable statistical models and high-performance computing algorithms for such models will be of substantial interest to statisticians and environmental scientists.

ACKNOWLEDGEMENTS

The work of the authors have been supported in part by National Science Foundation (NSF) under grants NSF/DMS 1916349 and NSF/IIS 1562303, and by the National Institute of Environmental Health Sciences (NIEHS) under grants R01ES030210 and 5R01ES027027.

SUPPLEMENTARY MATERIALS

The MODIS vegetation indices data analyzed in Section V, and the Julia code implementing our models are available at https://github.com/LuZhangstat/Multi_NNGP.

REFERENCES

Banerjee, S. (2017). “High-Dimensional Bayesian Geostatistics.” *Bayesian Analysis*, 12: 583–614.

-
- Banerjee, S., Carlin, B. P., and Gelfand, A. E. (2014). *Hierarchical modeling and analysis for spatial data*. CRC Press, Boca Raton, FL.
- Bezanson, J., Edelman, A., Karpinski, S., and Shah, V. B. (2017). "Julia: A fresh approach to numerical computing." *SIAM review*, 59(1): 65–98.
URL <https://doi.org/10.1137/141000671>
- Bourgault, G. and Marcotte, D. (1991). "Multivariable variogram and its application to the linear model of coregionalization." *Mathematical Geology*, 23(7): 899–928.
- Brown, P. J., Le, N. D., and Zidek, J. V. (1994). "Multivariate spatial interpolation and exposure to air pollutants." *Canadian Journal of Statistics*, 22(4): 489–509.
- Chilés, J. and Delfiner, P. (1999). *Geostatistics: Modeling Spatial Uncertainty*. John Wiley: New York.
- Chiles, J.-P. and Delfiner, P. (2009). *Geostatistics: modeling spatial uncertainty*, volume 497. John Wiley & Sons.
- Cressie, N. (1993). *Statistics for Spatial Data*. Wiley-Interscience, revised edition.
- Cressie, N. and Wikle, C. K. (2015). *Statistics for spatio-temporal data*. John Wiley & Sons, Hoboken, NJ.
- Datta, A., Banerjee, S., Finley, A. O., and Gelfand, A. E. (2016a). "Hierarchical Nearest-Neighbor Gaussian Process Models for Large Geostatistical Datasets." *Journal of the American Statistical Association*, 111: 800–812.
URL <http://dx.doi.org/10.1080/01621459.2015.1044091>
- Datta, A., Banerjee, S., Finley, A. O., Hamm, N. A. S., and Schaap, M. (2016b). "Non-separable Dynamic Nearest-Neighbor Gaussian Process Models for Large spatio-temporal Data With an Application to Particulate Matter Analysis." *Annals of Applied Statistics*, 10: 1286–1316.
URL <http://dx.doi.org/10.1214/16-A0AS931>
- Dawid, A. P. (1981). "Some matrix-variate distribution theory: Notational considerations and a Bayesian application." *Biometrika*, 68(1): 265–274.
URL <https://doi.org/10.1093/biomet/68.1.265>
- Eicker, F. (1963). "Asymptotic normality and consistency of the least squares estimators for families of linear regressions." *The Annals of Mathematical Statistics*, 447–456.
- Finley, A. O., Banerjee, S., and Carlin, B. P. (2007). "spBayes: an R package for univariate and multivariate hierarchical point-referenced spatial models." *Journal of statistical software*, 19(4): 1.
- Finley, A. O., Datta, A., Cook, B. C., Morton, D. C., Andersen, H. E., and Banerjee, S. (2019). "Efficient algorithms for Bayesian Nearest Neighbor Gaussian Processes." *Journal of Computational and Graphical Statistics*, 28(2): 401–414.
- Fong, D. C.-L. and Saunders, M. (2011). "LSMR: An iterative algorithm for sparse least-squares problems." *SIAM Journal on Scientific Computing*, 33(5): 2950–2971.
- Gamerman, D. and Moreira, A. R. (2004). "Multivariate spatial regression models." *Journal of multivariate analysis*, 91(2): 262–281.

-
- Gelfand, A., Schmidt, A., Banerjee, S., and C., S. (2004). "Nonstationary multivariate process modeling through spatially varying coregionalization." *TEST: An Official Journal of the Spanish Society of Statistics and Operations Research*, 13(2): 263–312.
URL <http://EconPapers.repec.org/RePEc:spr:testjl:v:13:y:2004:i:2:p:263-312>
- Gelfand, A. E. and Banerjee, S. (2010). "Multivariate Spatial Process Models." In Gelfand, A., Diggle, P., Fuentes, M., and Guttorp, P. (eds.), *Handbook of Spatial Statistics*, 495–516. Boca Raton, FL: CRC Press.
- Gelman, A., Carlin, J. B., Stern, H. S., Dunson, D. B., Vehtari, A., and Rubin, D. B. (2013). *Bayesian Data Analysis, 3rd Edition*. Chapman & Hall/CRC Texts in Statistical Science. Chapman & Hall/CRC.
- Genton, M. G. and Kleiber, W. (2015). "Cross-covariance functions for multivariate geostatistics." *Statistical Science*, 147–163.
- Gneiting, T. and Raftery, A. E. (2007). "Strictly proper scoring rules, prediction, and estimation." *Journal of the American Statistical Association*, 102(477): 359–378.
- Haario, H., Saksman, E., and Tamminen, J. (2005). "Componentwise adaptation for high dimensional MCMC." *Computational Statistics*, 20(2): 265–273.
- Heaton, M. J., Datta, A., Finley, A. O., Furrer, R., Guinness, J., Guhaniyogi, R., Gerber, F., Gramacy, R. B., Hammerling, D., Katzfuss, M., et al. (2019). "A case study competition among methods for analyzing large spatial data." *Journal of Agricultural, Biological and Environmental Statistics*, 24(3): 398–425.
- Katzfuss, M. (2017). "A multi-resolution approximation for massive spatial datasets." *Journal of the American Statistical Association*, 112: 201–214.
URL <http://dx.doi.org/10.1080/01621459.2015.1123632>
- Le, N., Sun, L., and Zidek, J. V. (2001). "Spatial prediction and temporal backcasting for environmental fields having monotone data patterns." *Canadian Journal of Statistics*, 29(4): 529–554.
- Le, N. D., Sun, W., and Zidek, J. V. (1997). "Bayesian multivariate spatial interpolation with data missing by design." *Journal of the Royal Statistical Society: Series B (Statistical Methodology)*, 59(2): 501–510.
- Le, N. D. and Zidek, J. V. (2006). *Statistical analysis of environmental space-time processes*. Springer Science & Business Media.
- Lopes, H. F., Salazar, E., and Gamerman, D. (2008). "Spatial Dynamic Factor Analysis." *Bayesian Analysis*, 3(4): 759 – 792.
- Marshall, A. W. and Olkin, I. (1990). "Matrix versions of the Cauchy and Kantorovich inequalities." *Aequationes Mathematicae*, 40(1): 89–93.
- Mu, Q., Zhao, M., and Running, S. W. (2013). "MODIS global terrestrial evapotranspiration (ET) product (NASA MOD16A2/A3)." *Algorithm Theoretical Basis Document, Collection*, 5.
- Nishimura, A. and Suchard, M. A. (2018). "Prior-preconditioned conjugate gradient method for accelerated Gibbs sampling in" large n & large p sparse Bayesian regression." *arXiv preprint arXiv:1810.12437*.

-
- Ramon Solano, R., Didan, K., Jacobson, A., and Huete, A. (2010). "Modis Vegetation Index User's Guide." *The University of Arizona: Tucson, AZ, USA*.
- Ren, Q. and Banerjee, S. (2013). "Hierarchical factor models for large spatially misaligned datasets: A low-rank predictive process approach." *Biometrics*, 69: 19–30.
- Roberts, G. O. and Rosenthal, J. S. (2009). "Examples of adaptive MCMC." *Journal of Computational and Graphical Statistics*, 18(2): 349–367.
- Salvaña, M. L. O. and Genton, M. G. (2020). "Nonstationary cross-covariance functions for multivariate spatio-temporal random fields." *Spatial Statistics*, 100411.
- Schmidt, A. M. and Gelfand, A. E. (2003). "A Bayesian coregionalization approach for multivariate pollutant data." *Journal of Geophysical Research: Atmospheres*, 108(D24).
- Sulla-Menashe, D. and Friedl, M. A. (2018). "User guide to collection 6 MODIS land cover (MCD12Q1 and MCD12C1) product." *USGS: Reston, VA, USA*, 1–18.
- Sun, W., Le, N. D., Zidek, J. V., and Burnett, R. (1998). "Assessment of a Bayesian multivariate interpolation approach for health impact studies." *Environmetrics: The official journal of the International Environmetrics Society*, 9(5): 565–586.
- Sun, Y., Li, B., and Genton, M. (2011). "Geostatistics for large datasets." In Montero, J., Porcu, E., and Schlather, M. (eds.), *Advances And Challenges In Space-time Modelling Of Natural Events*, 55–77. Berlin Heidelberg: Springer-Verlag.
- Taylor-Rodriguez, D., Finley, A. O., Datta, A., Babcock, C., Andersen, H. E., Cook, B. D., Morton, D. C., and Banerjee, S. (2019). "Spatial factor models for high-dimensional and large spatial data: An application in forest variable mapping." *Statistica Sinica*, 29(3): 1155–1180.
- Thorndike, R. L. (1953). "Who belongs in the family." In *Psychometrika*. Citeseer.
- Wackernagel, H. (2003). *Multivariate Geostatistics*. Springer-Verlag, Berlin, 3 edition.
- Wang, F. and Wall, M. M. (2003). "Generalized common spatial factor model." *Biostatistics*, 4(4): 569–582.
URL <http://dx.doi.org/10.1093/biostatistics/4.4.569>
- Zhang, L., Banerjee, S., and Finley, A. O. (2020). "High-dimensional multivariate Geostatistics: A Bayesian Matrix-Normal Approach." *arXiv preprint arXiv:2003.10051*.

S.1. ALGORITHM OF NNGP BASED BLMC MODEL

We discuss posterior predictive inference a detailed algorithm. Let $N_m(\mathbf{u}_i)$ be the m neighbors of $\mathbf{u}_i \in \mathcal{U}$ among \mathcal{S} . The posterior predictive distribution for $\mathbf{f}_k(\mathcal{U})$ given in (II.14) follows

$$\mathbf{f}_k(\mathcal{U}) \mid \mathbf{f}_k, \psi_k \sim \mathbf{N}(\tilde{\mathbf{A}}\mathbf{f}_k, \tilde{\mathbf{D}}), \quad (\text{S.1})$$

where the (i, j) -th entry of $\tilde{\mathbf{A}}$ is 0 when $\mathbf{s}_j \notin N_m(\mathbf{u}_i)$ and, similar to \mathbf{A}_{ρ_k} , the m nonzero entries in the i -th row of $\tilde{\mathbf{A}}$ are the $1 \times m$ vector $\tilde{\mathbf{a}}_i^\top = \boldsymbol{\rho}_{\psi_k}(\mathbf{u}_i, N_m(\mathbf{u}_i))\boldsymbol{\rho}_{\psi_k}(N_m(\mathbf{u}_i), N_m(\mathbf{u}_i))^{-1}$. The (i, i) -th

diagonal element of $\tilde{\mathbf{D}}$ equals $\rho_{\psi_k}(\mathbf{u}_i, \mathbf{u}_i) - \tilde{\mathbf{a}}_i^\top \boldsymbol{\rho}_{\psi_k}(N_m(\mathbf{u}_i), \mathbf{u}_i)$. The posterior sample of $\mathbf{Y}_{\mathcal{U}}$ after giving posterior sample of $\boldsymbol{\beta}, \boldsymbol{\Lambda}, \boldsymbol{\Sigma}$ and $\mathbf{F}_{\mathcal{U}}$ can be sampled through

$$\text{MN}(\mathbf{X}_{\mathcal{U}}\boldsymbol{\beta} + \mathbf{F}_{\mathcal{U}}\boldsymbol{\Lambda}, \mathbf{I}_{n'}, \boldsymbol{\Sigma}) . \quad (\text{S.2})$$

The following gives the detailed algorithm.

Algorithm 1: Obtaining posterior inference of $\{\gamma, \boldsymbol{\Sigma}, \omega\}$ and predictions on a new set \mathcal{U} for NNGP based BLMC model

1. Precalculation and preallocation for the MCMC algorithm
 - (a) Find location sets \mathcal{S}, \mathcal{M} and the index of the observed and missing response $\{os_i\}_{i=1}^n$ and $\{ms_i\}_{i=1}^n$.
 - (b) Build the nearest neighbor for \mathcal{S}
 - (c) Calculate Cholesky decompositions $\mathbf{V}_{\boldsymbol{\Lambda}} = \mathbf{L}_{\boldsymbol{\Lambda}}\mathbf{L}_{\boldsymbol{\Lambda}}^\top$ and $\mathbf{V}_{\boldsymbol{\beta}} = \mathbf{L}_{\boldsymbol{\beta}}\mathbf{L}_{\boldsymbol{\beta}}^\top$
 - (d) Preallocate MCMC samples and initialize MCMC chain with $\boldsymbol{\beta}^{(0)}, \boldsymbol{\Lambda}^{(0)}, \boldsymbol{\Sigma}^{(0)}$ and $\{\psi_k^{(0)}\}_{k=1}^K$
2. Block update MCMC algorithm. For $l = 1 : L$
 - (a) Update $\mathbf{F}^{(l)}$ and impute missing response $\{\mathbf{y}(\mathbf{s}_i)_{ms_i}^{(l)}\}_{\mathbf{s}_i \in \mathcal{M}}$
 - Construct $\tilde{\mathbf{X}}$ and $\tilde{\mathbf{Y}}$ in (II.7)
 - Build the matrix $\mathbf{D}_{\boldsymbol{\Sigma}^o}^{\frac{1}{2}} = \text{diag}(\{\boldsymbol{\Sigma}_{os_i}^{-\frac{1}{2}}\}_{i=1}^n)$ in (II.7) $\mathcal{O}(n)$
 - Construct $\{\mathbf{A}_{\rho_k}\}_{k=1}^K$ and $\{\mathbf{D}_{\rho_k}\}_{k=1}^K$ as described, for example, in Finley et al. (2019) $\mathcal{O}(Knm^3)$
 - Construct $\tilde{\mathbf{X}}$ and $\tilde{\mathbf{Y}}$ in (II.7) with $\mathbf{V}_k = \mathbf{D}_{\rho_k}^{-\frac{1}{2}}(\mathbf{I} - \mathbf{A}_{\rho_k})$ $\mathcal{O}(nK(m+1+q) + npq)$
 - Use LSMR (Fong and Saunders, 2011) to generate sample of $\mathbf{F}^{(l)}$
 - Sample $\mathbf{u} \sim \mathbf{N}(\mathbf{0}, \mathbf{I}_{Kn})$ $\mathcal{O}(nK)$
 - Solve $\text{vec}(\mathbf{F})^{(l)}$ from $\tilde{\mathbf{X}}\text{vec}(\mathbf{F})^{(l)} = \tilde{\mathbf{Y}} + \mathbf{u}$ by LSMR
 - Impute missing response $\{\mathbf{y}(\mathbf{s}_i)_{ms_i}^{(l)}\}_{\mathbf{s}_i \in \mathcal{M}}$ over \mathcal{M} through (II.9)
 - Calculate $\boldsymbol{\mu}_{\mathbf{s}} = \boldsymbol{\beta}^{(l)\top} \mathbf{x}(\mathbf{s}) + \boldsymbol{\Lambda}^{(l-1)} \mathbf{f}(\mathbf{s})$ for $\mathbf{s} \in \mathcal{M}$
 - Sample $\mathbf{y}(\mathbf{s})_{ms}^{(l)}$ by (II.9) for $\mathbf{s} \in \mathcal{M}$
 - (b) Use MNIW to update $\{\boldsymbol{\beta}^{(l)}, \boldsymbol{\Lambda}^{(l)}, \boldsymbol{\Sigma}^{(l)}\}$
 - Construct \mathbf{X}^* and \mathbf{Y}^* in (II.10)
 - Generate $\boldsymbol{\Sigma}^{(l)}$
 - (When $\boldsymbol{\Sigma}$ is a positive symmetric matrix)
 - * Calculate $\boldsymbol{\mu}^*, \mathbf{V}^{*-1}, \boldsymbol{\Psi}^*$ and ν^* by (II.11) $\mathcal{O}(n(p+K)(p+K+q))$
 - * Sample $\boldsymbol{\Sigma}^{(l)}$ from $\text{IW}(\boldsymbol{\Psi}, \nu^*)$
 - (When $\boldsymbol{\Sigma}$ is diagonal)
 - * Calculate $\boldsymbol{\mu}^*$ by (II.11) $\mathcal{O}(n(p+K)(p+K+q))$
 - * Sample elements of $\boldsymbol{\Sigma}^{(l)}$ from Inverse-Gamma with parameters provided in (II.12)
 - Sample $\boldsymbol{\gamma}^{(l)} = [\boldsymbol{\beta}^{(l)\top}, \boldsymbol{\Lambda}^{(l)\top}]^\top$ from $\text{MN}(\boldsymbol{\mu}^*, \mathbf{V}^*, \boldsymbol{\Sigma}^{(l)})$
 - i. Sample $\mathbf{u} \sim \text{MN}(\mathbf{0}, \mathbf{I}_{p+K}, \mathbf{I}_q)$
 - ii. Calculate Cholesky decomposition $\mathbf{V}^{*-1} = \mathbf{L}_{\mathbf{V}}\mathbf{L}_{\mathbf{V}}^\top$ and $\boldsymbol{\Sigma}^{(l)} = \mathbf{L}_{\boldsymbol{\Sigma}^{(l)}}\mathbf{L}_{\boldsymbol{\Sigma}^{(l)}}^\top$
 - iii. Generate $\boldsymbol{\gamma}^{(l)} = \boldsymbol{\mu}^* + \mathbf{L}_{\mathbf{V}}^{-\top} \mathbf{u}\mathbf{L}_{\boldsymbol{\Sigma}^{(l)}}^\top$
 - (c) Use Metropolis random walk to update $\{\boldsymbol{\Psi}_k^{(l)}\}_{k=1}^K$
 - i. Propose new $\{\boldsymbol{\Psi}_k^*\}_{k=1}^K$ based on $\{\boldsymbol{\Psi}_k^{(l-1)}\}_{k=1}^K$
 - ii. Calculate the likelihood of the new proposed $\{\boldsymbol{\Psi}_k^*\}_{k=1}^K$ and $\{\boldsymbol{\Psi}_k^{(l-1)}\}_{k=1}^K$ given $\mathbf{F}^{(l)}$ using (II.13) $\mathcal{O}(Knm^3)$
 - iii. Accept the new $\{\boldsymbol{\Psi}_k^*\}_{k=1}^K$ as $\{\boldsymbol{\Psi}_k^{(l)}\}_{k=1}^K$ with the probability of the ratio of the likelihood of $\{\boldsymbol{\Psi}_k^*\}_{k=1}^K$ and $\{\boldsymbol{\Psi}_k^{(l-1)}\}_{k=1}^K$. Let $\{\boldsymbol{\Psi}_k^{(l)}\}_{k=1}^K = \{\boldsymbol{\Psi}_k^{(l-1)}\}_{k=1}^K$ when the new proposal is rejected.
3. Generate posterior samples of $\{\mathbf{F}_{\mathcal{U}}^{(l)}, \mathbf{Y}_{\mathcal{U}}^{(l)}\}$ on a new set \mathcal{U}

-
- (a) Construct $\tilde{\mathbf{A}}$ and $\tilde{\mathbf{D}}$ in (S.1) $\mathcal{O}(n'm^3K)$
 - (b) Generate $\mathbf{f}_k(\mathcal{U})^{(l)} \sim \mathcal{N}(\tilde{\mathbf{A}}\mathbf{f}_k, \tilde{\mathbf{D}})$ for $k = 1, \dots, K$ $\mathcal{O}(n'Km)$
 - (c) Sample $\mathbf{Y}_{\mathcal{U}}^{(l)} \mid \omega_{\mathcal{U}}^{(l)}, \gamma^{(l)}, \Sigma^{(l)}, \mathbf{F}_{\mathcal{U}}^{(l)} \sim \text{MN}(\mathbf{X}_{\mathcal{U}}\boldsymbol{\beta} + \mathbf{F}_{\mathcal{U}}\boldsymbol{\Lambda} + \mathbf{I}_{n'}, \Sigma^{(l)})$
- Sample $\mathbf{u} \sim \text{MN}(\mathbf{0}, \mathbf{I}_{n'}, \mathbf{I}_q)$ $\mathcal{O}(n'q)$
 - Generate $\mathbf{Y}_{\mathcal{U}}^{(l)} = \mathbf{X}_{\mathcal{U}}\boldsymbol{\beta} + \mathbf{F}_{\mathcal{U}}\boldsymbol{\Lambda} + \mathbf{u}\mathbf{L}_{\Sigma^{(l)}}^{-1}$ with $\mathbf{F}_{\mathcal{U}}^{(l)} = [f_1(\mathcal{U})^{(l)} : \dots : f_K(\mathcal{U})^{(l)}]$ $\mathcal{O}(n'(pq + Kq + q^2))$
-

S.2. TECHNICAL DETAILS AND PROOFS OF RESULTS IN SECTION III

Let us begin with a representation of posterior distributions of the latent model in Section III. Let \mathbf{V}_ρ be a non-singular square matrix such that $\rho_\psi^{-1}(\mathcal{S}, \mathcal{S}) = \mathbf{V}_\rho^\top \mathbf{V}_\rho$. Treat the prior of γ as additional observations and recast $p(\mathbf{Y}, \gamma \mid \Sigma) = p(\mathbf{Y} \mid \gamma, \Sigma) \times p(\gamma \mid \Sigma)$ into an augmented linear model

$$\underbrace{\begin{bmatrix} \sqrt{\frac{\alpha}{1-\alpha}}\mathbf{Y} \\ \mathbf{L}_r^{-1}\boldsymbol{\mu}_\beta \\ \mathbf{0} \end{bmatrix}}_{\mathbf{Y}^*} = \underbrace{\begin{bmatrix} \sqrt{\frac{\alpha}{1-\alpha}}\mathbf{X} & \sqrt{\frac{\alpha}{1-\alpha}}\mathbf{I}_n \\ \mathbf{L}_r^{-1} & \mathbf{0} \\ \mathbf{0} & \mathbf{V}_\rho \end{bmatrix}}_{\mathbf{X}^*} \underbrace{\begin{bmatrix} \boldsymbol{\beta} \\ \boldsymbol{\omega} \end{bmatrix}}_{\boldsymbol{\gamma}} + \underbrace{\begin{bmatrix} \eta_1 \\ \eta_2 \\ \eta_3 \end{bmatrix}}_{\boldsymbol{\eta}}, \quad (\text{S.1})$$

where \mathbf{L}_r is the Cholesky decomposition of \mathbf{V}_r , and $\boldsymbol{\eta} \sim \text{MN}(\mathbf{0}, \mathbf{I}_{2n+p}, \Sigma)$. When having a flat prior for $\boldsymbol{\beta}$, \mathbf{L}_r^{-1} degenerates to a zero matrix, showing no information from $\boldsymbol{\beta}$'s prior contributes to the linear system. The expression in (III.5) can be simplified as

$$\begin{aligned} \mathbf{V}^* &= (\mathbf{X}^{*\top} \mathbf{X}^*)^{-1}, \quad \boldsymbol{\mu}^* = (\mathbf{X}^{*\top} \mathbf{X}^*)^{-1} \mathbf{X}^{*\top} \mathbf{Y}^*, \\ \boldsymbol{\Psi}^* &= \boldsymbol{\Psi} + (\mathbf{Y}^* - \mathbf{X}^* \boldsymbol{\mu}^*)^\top (\mathbf{Y}^* - \mathbf{X}^* \boldsymbol{\mu}^*), \quad v^* = v + n. \end{aligned} \quad (\text{S.2})$$

We explore the behavior of the above posterior density as the number of observations becomes large under a true data generating distribution. Assume that the true distribution of the dependent variables is included in the parametric family $f(\mathbf{Y}) = p(\mathbf{Y} \mid \boldsymbol{\beta}_0, \Sigma_0)$ for some Σ_0 and $\boldsymbol{\beta}_0$. For distinguishing the variables based on the number of observations, we make the dependence upon n explicit. Denote $\mathbf{X}(n)_{n \times p} = [\mathbf{x}(\mathbf{s}_1) : \dots : \mathbf{x}(\mathbf{s}_n)]^\top$, $\mathbf{Y}(n)_{n \times q} = [\mathbf{y}(\mathbf{s}_1) : \dots : \mathbf{y}(\mathbf{s}_n)]^\top$, $\mathcal{S}(n) = \{\mathbf{s}_1, \dots, \mathbf{s}_n\}$, $\mathcal{K}(n) = \mathbf{C}(\mathcal{S}(n), \mathcal{S}(n)) + (\alpha^{-1} - 1)\mathbf{I}_n$. $\mathbf{X}^*(n)$ and $\mathbf{Y}^*(n)$ are \mathbf{X}^* and \mathbf{Y}^* in (S.1) using $\mathbf{X}(n)$ and $\mathbf{Y}(n)$ instead of \mathbf{X} and \mathbf{Y} .

Lemma S.1. *The matrix Σ in the conjugate multivariate models is posterior consistent if and only if $\boldsymbol{\Psi}^*(n)_{ij}/n \rightarrow \{\Sigma_0\}_{ij}$ a.s. for $1 \leq i, j \leq q$ with $\boldsymbol{\Psi}^*(n)$ defined by (III.3) & (III.5)*

Proof. The conjugate multivariate models yield $\Sigma \mid \mathbf{Y}(n) \sim \text{IW}(\boldsymbol{\Psi}^*(n), v^*(n))$ with

$$\mathbf{M}_{ij} = \mathbb{E}(\Sigma_{ij} \mid \mathbf{Y}(n)) = \frac{\boldsymbol{\Psi}^*(n)_{ij}}{c-1}, \quad \text{Var}(\Sigma_{ij} \mid \mathbf{Y}(n)) = \frac{(c+1)\boldsymbol{\Psi}^*(n)_{ij}^2 + (c-1)\boldsymbol{\Psi}^*(n)_{ii}\boldsymbol{\Psi}^*(n)_{jj}}{c(c-1)^2(c-3)},$$

where $c = v^*(n) - p$, $\boldsymbol{\Psi}^*(n)$ and $v^*(n)$ are defined in (III.3) and (III.5) for the response and latent process models, respectively.

Necessity: If Σ is posterior consistent, i.e., for any $\epsilon > 0$

$$\lim_{n \rightarrow \infty} \Pr(|\Sigma_{ij} - \Sigma_{0ij}| > \epsilon \mid \mathbf{Y}(n)) = 0 \text{ for } 1 \leq i, j \leq q,$$

then $\lim_{n \rightarrow \infty} \mathbb{E}(\boldsymbol{\Sigma}_{ij} - \boldsymbol{\Sigma}_{0ij} | \mathbf{Y}(n)) \leq \lim_{n \rightarrow \infty} \mathbb{E}(|\boldsymbol{\Sigma}_{ij} - \boldsymbol{\Sigma}_{0ij}| | \mathbf{Y}(n)) < \epsilon$ for any $\epsilon > 0$; hence, $\lim_{n \rightarrow \infty} \mathbb{E}(\boldsymbol{\Sigma}_{ij} | \mathbf{Y}(n)) = \boldsymbol{\Sigma}_{0ij}$ a.s. Therefore, $\boldsymbol{\Psi}^*(n)_{ij}/n \rightarrow \boldsymbol{\Sigma}_{0ij}$ a.s. for $1 \leq i, j \leq q$.

Sufficiency: If $\boldsymbol{\Psi}^*(n)_{ij}/n \rightarrow \boldsymbol{\Sigma}_{0ij}$ a.s. for $1 \leq i, j \leq q$, then, from the posterior distribution of $\boldsymbol{\Sigma}$ directly obtain $\lim_{n \rightarrow \infty} \mathbb{E}(\boldsymbol{\Sigma}_{ij} | \mathbf{Y}(n)) = \boldsymbol{\Sigma}_{0ij}$ and the variance of each element converges to 0 at the rate of $1/n$. Using the triangle and Chebyshev's inequalities, for any $\epsilon > 0$ we obtain $\Pr(|\boldsymbol{\Sigma}_{ij} - \boldsymbol{\Sigma}_{0ij}| > \epsilon | \mathbf{Y}(n)) \leq \Pr(|\boldsymbol{\Sigma}_{ij} - \mathbf{M}_{ij}| > \epsilon/2 | \mathbf{Y}(n)) + \Pr(|\mathbf{M}_{ij} - \boldsymbol{\Sigma}_{0ij}| > \epsilon/2 | \mathbf{Y}(n)) \leq 4\text{Var}(\boldsymbol{\Sigma}_{ij} | \mathbf{Y}(n))/\epsilon^2 + \Pr(|\mathbf{M}_{ij} - \boldsymbol{\Sigma}_{0ij}| > \epsilon/2 | \mathbf{Y}(n)) \rightarrow 0$ a.s. \square

Theorem S.2. *The matrix $\boldsymbol{\Sigma}$ in the conjugate multivariate models is posterior consistent.*

Proof. From (S.1), it follows that $\mathbf{u}(n) | \boldsymbol{\Sigma}_0 \sim \text{MN}_{(2n+p) \times q}(\mathbf{0}, \mathbf{I}_{2n+p}, \boldsymbol{\Sigma}_0)$, where $\mathbf{u}(n) = \mathbf{Y}^*(n) - \mathbf{X}^*(n)\boldsymbol{\gamma}$ and we write $\boldsymbol{\Psi}^*(n)/n = \boldsymbol{\Psi}/n + \frac{1}{n}\mathbf{u}(n)^\top (\mathbf{I}_n - \mathbf{H}^*(n)) \mathbf{u}(n)$, where $\mathbf{H}^*(n) = \mathbf{X}^*(n)(\mathbf{X}^*(n)^\top \mathbf{X}^*(n))^{-1} \mathbf{X}^*(n)^\top$ is idempotent with rank $p+n$. Writing $\mathbf{H}^*(n) = \mathbf{Q}(n)^\top \tilde{\mathbf{I}} \mathbf{Q}(n)$, where $\mathbf{Q}(n)$ is an orthogonal matrix and $\tilde{\mathbf{I}} = \begin{bmatrix} \mathbf{I}_{p+n} & \mathbf{O} \\ \mathbf{O} & \mathbf{O} \end{bmatrix}$ and letting $\mathbf{v}(n) = \mathbf{Q}(n)\mathbf{u}$, we obtain $\mathbf{v}(n) \sim \text{MN}_{(2n+p) \times q}(\mathbf{0}, \mathbf{I}_{2n+p}, \boldsymbol{\Sigma}_0)$. Also, we know $\lim_{n \rightarrow \infty} \frac{2}{2n} \{\mathbf{u}(n)^\top \mathbf{u}(n)\}_{ij} = 2\boldsymbol{\Sigma}_{0ij}$ a.s. for $1 \leq i, j, \leq q$ and $\lim_{n \rightarrow \infty} \frac{1}{n} \{\mathbf{u}(n)^\top \mathbf{H}^*(n) \mathbf{u}(n)\}_{ij} = \lim_{n \rightarrow \infty} \frac{1}{n} \sum_{l=1}^p \{\mathbf{v}_l^\top \mathbf{v}_l\}_{ij} = \boldsymbol{\Sigma}_{0ij}$ a.s. from the Khinchin-Kolmogorov strong law of large numbers, where \mathbf{v}_j is the j -th column of $\mathbf{v}(n)$. Hence, $\lim_{n \rightarrow \infty} \boldsymbol{\Psi}^*(n)_{ij}/n = \boldsymbol{\Sigma}_{0ij}$ a.s. and the result follows from Lemma S.1. \square

Theorem S.3. *The regression slopes $\boldsymbol{\beta}$ is posterior consistent for both conjugate models if and only if $\lim_{n \rightarrow \infty} \lambda_{\min}(\mathbf{P}(n)) = \infty$, where $\lambda_{\min}(\mathbf{P}(n))$ is the smallest eigenvalue of $\mathbf{P}(n)$.*

Proof. The augmented linear system (S.1) implies that the marginal posterior mean of $\boldsymbol{\beta}$ is an unbiased estimator of $\boldsymbol{\beta}_0$ with respect to the true distribution of $\mathbf{Y}(n)$. When $\boldsymbol{\beta}$ is posterior consistent, $\lim_{n \rightarrow \infty} \text{Var}(\boldsymbol{\beta}_{ij} | \mathbf{Y}(n)) = 0$ a.s with respect to the true distribution of $\mathbf{Y}(n)$. Moreover, $\lim_{n \rightarrow \infty} \text{Var}(\boldsymbol{\beta}_{ij} | \mathbf{Y}(n)) = 0$ a.s. is a sufficient condition for the posterior consistency of $\boldsymbol{\beta}$ through Chebyshev's inequality. In the conjugate model, $\boldsymbol{\beta} | \mathbf{Y}(n) \sim \text{T}_{p,q}(v^*(n) - q + 1, \boldsymbol{\mu}^*(n), \mathbf{V}^*(n), \boldsymbol{\Psi}^*(n))$ with parameters given in (III.3). From Theorem III.1, $\lim_{n \rightarrow \infty} \boldsymbol{\Psi}^*(n)_{ij}/n = \boldsymbol{\Sigma}_{0ij}$ a.s. for $1 \leq i, j, \leq q$, hence $\lim_{n \rightarrow \infty} \text{Var}(\boldsymbol{\beta}_{ij} | \mathbf{Y}(n)) = 0$ a.s. if and only if $\lim_{n \rightarrow \infty} \{\mathbf{V}^*(n)\}_{ii} = 0$ for all $i = 1, \dots, q$. Following Eicker (1963) (see his proof of Theorem 1), the sufficient and necessary condition is $\lim_{n \rightarrow \infty} \lambda_{\min}(\mathbf{V}^{*-1}(n)) = \infty$. Since $\lambda_{\min}(\mathbf{P}(n)) + \lambda_{\max}(\mathbf{V}_r^{-1}) \geq \lambda_{\min}(\mathbf{V}^{*-1}(n)) = \lambda_{\min}(\mathbf{P}(n) + \mathbf{V}_r^{-1}) \geq \lambda_{\min}(\mathbf{P}(n))$, the condition simplifies to $\lim_{n \rightarrow \infty} \lambda_{\min}(\mathbf{P}(n)) = \infty$. \square

The following remarks reveal that the posterior consistency in Theorem III.1 satisfies with common conditions.

Remark S.4. $\lambda_{\min}(\mathbf{P}(n))$ is non-decreasing, and when $\boldsymbol{\beta}$ is posterior consistent, $\lim_{n \rightarrow \infty} \mathbf{P}(n)_{ii} = \infty$ since $\mathbf{P}(n)_{ii} \geq \lambda_{\min}(\mathbf{P}(n))$

Proof. Let $\mathbf{X}(n+1) = [\mathbf{X}(n)^\top, x_{n+1}]^\top$, $\mathcal{K}(n+1) = \begin{bmatrix} \mathcal{K}(n) & \mathcal{K}_{(n),n+1} \\ \mathcal{K}_{n+1,(n)} & \alpha^{-1} \end{bmatrix}$. Then

$$\begin{aligned} \mathbf{P}(n+1) &= [\mathbf{X}(n)^\top, x_{n+1}] \begin{bmatrix} \mathcal{K}(n) & \mathcal{K}_{(n),n+1} \\ \mathcal{K}_{n+1,(n)} & \alpha^{-1} \end{bmatrix}^{-1} \begin{bmatrix} \mathbf{X}(n) \\ x_{n+1} \end{bmatrix} \\ &= \mathbf{P}(n) + (\mathbf{X}(n)^\top \mathcal{K}(n)^\top \mathcal{K}_{(n),n+1} - x_{n+1}) d(\mathcal{K}_{n+1,(n)} \mathcal{K}(n) \mathbf{X}(n) - x_{n+1}) \\ &= \mathbf{P}(n) + \mathbf{A}(n), \end{aligned} \tag{S.3}$$

where $d = (\alpha^{-1} - \mathcal{K}_{n+1,(n)}\mathcal{K}(n)^{-1}\mathcal{K}_{(n),n+1}) > 0$ and $\mathbf{A}(n)$ is positive semi-definite symmetric matrix. Thus, $\lambda_{\min}(\mathbf{P}(n+1)) = \lambda_{\min}(\mathbf{P}(n) + \mathbf{A}(n)) \geq \lambda_{\min}(\mathbf{P}(n))$. \square

Remark S.5. When $\mathbf{X}(n) \sim MN(\mathbf{0}, \mathcal{K}(n), \Sigma^*)$ for some Σ^* , β is posterior consistent.

Proof. Let $\mathcal{K}(n)^{-\frac{1}{2}}$ be the square root of $\mathcal{K}(n)^{-1}$. Then, $\mathcal{K}(n)^{-\frac{1}{2}}\mathbf{X}(n) \sim MN(\mathbf{0}, \mathbf{I}_n, \Sigma^*)$ and the strong law of large numbers ensures $\lim_{n \rightarrow \infty} \{\frac{1}{n}\mathbf{P}(n)\}_{ij} = \Sigma_{ij}^*$ a.s. for $1 \leq i, j \leq p$. Hence, $\lambda_{\min}(\mathbf{P}(n)) \rightarrow \infty$. \square

Remark S.6. If $\mathbf{X}(n) \sim MN(\mathbf{0}, \mathbf{I}_n, \Sigma^*)$ for some Σ^* , then β is posterior consistent

Proof. For any n , there exists an orthogonal matrix $\mathbf{Q}(n)$ and a diagonal matrix $\mathbf{D}(n)$ with diagonal entries d_i for $i = 1, 2, \dots, n$ such that $\mathbf{C}(\mathcal{S}(n), \mathcal{S}(n)) = \mathbf{Q}(n)^\top \mathbf{D}(n) \mathbf{Q}(n)$. This yields

$$\begin{aligned} \mathbf{P}(n) &= \mathbf{X}(n)^\top \mathbf{Q}(n)^\top (\mathbf{D}(n) + (\alpha^{-1} - 1)\mathbf{I}_n)^{-1} \mathbf{Q}(n) \mathbf{X}(n) \\ &= \mathbf{Z}(n)^\top \text{diag} \left(\left\{ \frac{1}{d_i + (\alpha^{-1} - 1)} \right\}_{i=1}^n \right) \mathbf{Z}(n) = \sum_{i=1}^n \frac{1}{d_i + (\alpha^{-1} - 1)} \mathbf{z}_i \mathbf{z}_i^\top, \end{aligned} \quad (\text{S.4})$$

where $\mathbf{Z}(n) = [\mathbf{z}_1 : \dots : \mathbf{z}_n]^\top \sim MN(\mathbf{0}, \mathbf{I}_n, \Sigma^*)$ and $\sum_{i=1}^n d_i = n$, $d_i \geq 0, i = 1, \dots, n$. Letting $\mathbf{V}_i = \mathbf{z}_i \mathbf{z}_i^\top$ for $i = 1, \dots, n$ and applying the matrix version of Cauchy-Schwarz inequality (see, e.g., equation 4 in Marshall and Olkin, 1990) we obtain

$$\sum_{i=1}^n (d_i + (\alpha^{-1} - 1)) \sum_{i=1}^n \frac{1}{d_i + (\alpha^{-1} - 1)} \mathbf{V}_i \geq \left\{ \sum_{i=1}^n \sqrt{d_i + (\alpha^{-1} - 1)} \frac{\mathbf{V}_i^{\frac{1}{2}}}{\sqrt{d_i + (\alpha^{-1} - 1)}} \right\}^2,$$

where $\mathbf{V}_i^{\frac{1}{2}} \mathbf{V}_i^{\frac{1}{2}} = \mathbf{V}_i$, and, hence, $\mathbf{P}(n) \geq \alpha \left\{ \sum_{i=1}^n \mathbf{V}_i^{\frac{1}{2}} / \sqrt{n} \right\}^2$. Letting $\mathbf{V}_i = \mathbf{z}_i \mathbf{z}_i^\top = \lambda_i \mathbf{u}_i \mathbf{u}_i^\top$ where $\lambda_i = \mathbf{z}_i^\top \mathbf{z}_i = \|\mathbf{z}_i\|^2$ and $\mathbf{u}_i = \frac{\mathbf{z}_i}{\|\mathbf{z}_i\|}$, we have $\mathbf{V}_i^{\frac{1}{2}} = \sqrt{\lambda_i} \mathbf{u}_i \mathbf{u}_i^\top$. Changing n into np and rewriting $\sum_{i=1}^n \mathbf{V}_i^{\frac{1}{2}}$ into $\sum_{i=1}^n \sum_{k=1}^p \mathbf{V}_{ik}^{\frac{1}{2}}$, where $\{\sum_{k=1}^p \mathbf{V}_{ik}^{\frac{1}{2}}\}$ for each i is a full rank $p \times p$ matrix with probability 1, we obtain

$$\mathbf{P}(np) \geq \frac{\alpha}{p} \left\{ \frac{\sum_{i=1}^n \sum_{k=1}^p \sqrt{\lambda_{ik}} \mathbf{u}_{ik} \mathbf{u}_{ik}^\top}{\sqrt{n}} \right\}^2 \quad (\text{S.5})$$

We now argue that the smallest eigenvalue of the matrix on the right side goes to infinity as $n \rightarrow \infty$, which will imply that $\lambda_{\min}(\mathbf{P}(np)) \rightarrow \infty$. Since $\sum_{k=1}^p \mathbf{V}_{ik}^{\frac{1}{2}} = \sum_{k=1}^p \sqrt{\lambda_{ik}} \mathbf{u}_{ik} \mathbf{u}_{ik}^\top \sim \mathbf{W}_p(\Sigma^{*\frac{1}{2}}, p)$, where \mathbf{W}_p is Wishart distribution, $\{\mathbf{u}_{i1}, \dots, \mathbf{u}_{ip}\}$ make up the bases of the space \mathbb{R}^p with probability 1. For any $\mathbf{u} \in \mathcal{R}^p, \|\mathbf{u}\| = 1$, we have

$$\mathbf{u}^\top \sum_{k=1}^p \left(\sqrt{\lambda_{ik}} \mathbf{u}_{ik} \mathbf{u}_{ik}^\top \right) \mathbf{u} \geq \min_{k=1, \dots, p} \{ \sqrt{\lambda_{ik}} \}$$

Hence, $\lambda_{\min}(\sum_{i=1}^n \sum_{k=1}^p \sqrt{\lambda_{ik}} \mathbf{u}_{ik} \mathbf{u}_{ik}^\top) \geq \sum_{i=1}^n \min_{k=1, \dots, p} \{ \sqrt{\lambda_{ik}} \}$. Since $\lambda_{ik} = \|\mathbf{z}_{ik}\|^2$ where $\mathbf{z}_{ik} \sim N(\mathbf{0}, \Sigma^*)$, $\min_{k=1, \dots, p} \{ \sqrt{\lambda_{ik}} \}$ are independent and identically distributed with a positive mean $\mathbb{E}(\min_{k=1, \dots, p} \{ \sqrt{\lambda_{ik}} \}) = c^* > 0$ and a finite variance σ^{2*} . By law of large numbers, we have $\lim_{n \rightarrow \infty} \sum_{i=1}^n \min_{k=1, \dots, p} \{ \sqrt{\lambda_{ik}} \} / n =$

c^* a.s.. Therefore,

$$\lambda_{\min} \left(\left\{ \frac{\sum_{i=1}^n \sum_{k=1}^p \sqrt{\lambda_{ik}} \mathbf{u}_{ik} \mathbf{u}_{ik}^\top}{\sqrt{n}} \right\}^2 \right) \geq \frac{1}{n} \left\{ \sum_{i=1}^n \min_{k=1, \dots, p} \{ \sqrt{\lambda_{ik}} \} \right\}^2 \rightarrow \infty$$

By (S.5), $\lim_{n \rightarrow \infty} \lambda_{\min}(\mathbf{P}(n)) = \infty$. \square

S.3. MULTIVARIATE RESPONSE NNGP MODEL WITH MISALIGNMENT

The conjugacy in conjugate multivariate response model is violated with misalignment. Therefore, for datasets with misalignment, we need to drop data on the location with misalignment and use the ‘‘cleaned up’’ data to obtain quick inference through the conjugate model. However, for NNGP based response model, we can provide a modified algorithm that can utilize the ‘‘dropped’’ data to improve the inference of the conjugate multivariate response NNGP model.

Assume \mathcal{S} is the set of observed locations, where at least one response is recorded, $\mathcal{M}_i \subset \mathcal{S}$ is the set of locations where the i th response has not been observed. Let $\mathcal{M} = \cup \{\mathcal{M}_i\}_{i=1}^q$ and assume \mathcal{M} has n_m locations, then $\mathcal{R} = \mathcal{S} \setminus \mathcal{M}$ is the observed n_r locations with no misalignment. We label $\mathbf{Y}_{\mathcal{R}}$ and $\mathbf{X}_{\mathcal{R}}$ as the responses and design matrix over \mathcal{R} . The posterior distributions $p(\boldsymbol{\Sigma} | \mathbf{Y}_{\mathcal{R}})$ and $p(\boldsymbol{\beta} | \boldsymbol{\Sigma}, \mathbf{Y}_{\mathcal{R}})$ are given in (III.3) using \mathcal{R} instead of \mathcal{S} . For $\mathbf{s} \in \mathcal{M}$, we use footnote os to denote the index of observed responses on \mathbf{s} , the vector of observed responses on location \mathbf{s} is $\mathbf{y}(\mathbf{s})_{os}$ and the corresponding coefficient matrix is $\boldsymbol{\beta}_{os}$. Then, the posterior distribution of $\boldsymbol{\Sigma}$ given all observed data is

$$\begin{aligned} p(\boldsymbol{\Sigma} | \mathbf{Y}_{\mathcal{R}}, \{\mathbf{y}(\mathbf{s})_{os}\}_{\mathbf{s} \in \mathcal{M}}) &\propto \int p(\{\mathbf{y}(\mathbf{s})_{os}\}_{\mathbf{s} \in \mathcal{M}} | \boldsymbol{\Sigma}, \boldsymbol{\beta}, \mathbf{Y}_{\mathcal{R}}) p(\boldsymbol{\beta} | \boldsymbol{\Sigma}, \mathbf{Y}_{\mathcal{R}}) d\boldsymbol{\beta} p(\boldsymbol{\Sigma} | \mathbf{Y}_{\mathcal{R}}) \\ &\propto p(\{\mathbf{y}(\mathbf{s})_{os}\}_{\mathbf{s} \in \mathcal{M}} | \boldsymbol{\Sigma}, \mathbf{Y}_{\mathcal{R}}) p(\boldsymbol{\Sigma} | \mathbf{Y}_{\mathcal{R}}). \end{aligned} \quad (\text{S.1})$$

Now consider the formulation of $p(\{\mathbf{y}(\mathbf{s})_{os}\}_{\mathbf{s} \in \mathcal{M}} | \boldsymbol{\Sigma}, \mathbf{Y}_{\mathcal{R}})$. Let \mathcal{R} be the reference set for the response processes. Define the m nearest neighbor of \mathbf{s} in \mathcal{R} as $N_m(\mathbf{s})$ and $n_{\mathcal{R}}$ as the number of locations in \mathcal{R} , we have

$$p(\{\mathbf{y}(\mathbf{s})_{os}\}_{\mathbf{s} \in \mathcal{M}} | \boldsymbol{\Sigma}, \boldsymbol{\beta}, \mathbf{Y}_{\mathcal{R}}) = \prod_{\mathbf{s} \in \mathcal{M}} \mathcal{N}(\mathbf{y}(\mathbf{s})_{os} | \text{vec}[\mathbf{x}(\mathbf{s})^\top \boldsymbol{\beta} + \mathbf{L}_{\mathbf{s}}^\top \{\mathbf{Y}_{\mathcal{R}} - \mathbf{X}_{\mathcal{R}} \boldsymbol{\beta}\}]_{os}, \mathbf{D}_{\mathbf{s}}),$$

where $\mathbf{L}_{\mathbf{s}}$ is a $n_{\mathcal{R}} \times 1$ vector whose i -th element is zero if $\mathbf{s}_i \notin N_m(\mathbf{s})$. Define the index of nonzero elements in $\mathbf{L}_{\mathbf{s}}$ as $\text{Pa}[\mathbf{s}]$, then we have

$$\begin{aligned} \mathbf{L}_{\mathbf{s}}[\text{Pa}[\mathbf{s}]] &= [\mathcal{K}(\mathbf{s}, N_m(\mathbf{s})) \mathcal{K}(N_m(\mathbf{s}), N_m(\mathbf{s}))^{-1}]^\top, \\ \mathbf{D}_{\mathbf{s}} &= [\mathcal{K}(\mathbf{s}, \mathbf{s}) - \mathcal{K}(\mathbf{s}, N_m(\mathbf{s})) \mathcal{K}(N_m(\mathbf{s}), N_m(\mathbf{s}))^{-1} \mathcal{K}(N_m(\mathbf{s}), \mathbf{s})] \boldsymbol{\Sigma}_{[os, os]} \end{aligned} \quad (\text{S.2})$$

where $\boldsymbol{\Sigma}_{[os, os]}$ denotes the sub-matrix extracted from $\boldsymbol{\Sigma}$ with row and column index os . Let $\boldsymbol{\beta} | \boldsymbol{\Sigma}, \mathbf{Y}_{\mathcal{R}} \sim \text{MN}(\boldsymbol{\mu}^*, \mathbf{V}^*, \boldsymbol{\Sigma})$ and define $\mathbf{V}_{pr} = \boldsymbol{\Sigma} \otimes \mathbf{V}^*$, by intergrating out $\boldsymbol{\beta}$ we have

$$\{\mathbf{y}(\mathbf{s})_{os}\}_{\mathbf{s} \in \mathcal{M}} | \boldsymbol{\Sigma}, \mathbf{Y}_{\mathcal{R}} \sim \mathcal{N}(\mathbf{H}_1 \text{vec}(\boldsymbol{\mu}^*) + \mathbf{H}_2 \text{vec}(\mathbf{Y}_{\mathcal{R}}), \text{diag}(\{\mathbf{D}_{\mathbf{s}}\}_{\mathbf{s} \in \mathcal{M}}) + \mathbf{H}_1 \mathbf{V}_{pr} \mathbf{H}_1^\top), \quad (\text{S.3})$$

where

$$\begin{aligned} \mathbf{H}_1 &= \{\mathbf{I}_{q[os, :]} \otimes \mathbf{x}(\mathbf{s})^\top\}_{\mathbf{s} \in \mathcal{M}} - \mathbf{H}_2 [\mathbf{I}_q \otimes \mathbf{X}_{\mathcal{R}}], \\ \mathbf{H}_2 &= \{\mathbf{I}_{q[os, :]} \otimes \mathbf{L}_{\mathbf{s}}^\top\}_{\mathbf{s} \in \mathcal{M}}. \end{aligned} \quad (\text{S.4})$$

Here, $\mathbf{I}_{q[os,:]}$ is the $osth$ row of a $q \times q$ identity matrix, thus \mathbf{H}_2 provides the index of observed response and weights of neighbors for $\mathbf{s} \in \mathcal{M}$. Once q and p are relatively small, we can use matrix determinant lemma and Sherman-Morrison-Woodbury formulas

$$\begin{aligned} \det(\text{diag}(\{\mathbf{D}_s\}_{s \in \mathcal{M}}) + \mathbf{H}_1 \mathbf{V}_{pr} \mathbf{H}_1^\top) &= \det(\mathbf{V}_{update}) \det(\mathbf{V}_{pr}) \prod_{s \in \mathcal{M}} \det(\mathbf{D}_s) ; \\ (\text{diag}(\{\mathbf{D}_s\}_{s \in \mathcal{M}}) + \mathbf{H}_1 \mathbf{V}_{pr} \mathbf{H}_1^\top)^{-1} &= \text{diag}(\{\mathbf{D}_s^{-1}\}_{s \in \mathcal{M}}) - \\ &\quad \text{diag}(\{\mathbf{D}_s^{-1}\}_{s \in \mathcal{M}}) \mathbf{H}_1 \mathbf{V}_{update}^{-1} \mathbf{H}_1^\top \text{diag}(\{\mathbf{D}_s^{-1}\}_{s \in \mathcal{M}}) , \end{aligned} \quad (\text{S.5})$$

with $\mathbf{V}_{update} = \mathbf{V}_{pr}^{-1} + \mathbf{H}_1^\top \text{diag}(\{\mathbf{D}_s^{-1}\}_{s \in \mathcal{M}}) \mathbf{H}_1$ to facilitate the calculation of $p(\{\mathbf{y}(\mathbf{s})_{os}\}_{s \in \mathcal{M}} | \boldsymbol{\Sigma}, \mathbf{Y}_{\mathcal{R}})$. Plugging the above two equations into the log-likelihood of $\{\mathbf{y}(\mathbf{s})_{os}\}_{s \in \mathcal{M}} | \boldsymbol{\Sigma}, \mathbf{Y}_{\mathcal{R}}$

$$\begin{aligned} \log\{p(\{\mathbf{y}(\mathbf{s})_{os}\}_{s \in \mathcal{M}} | \boldsymbol{\Sigma}, \mathbf{Y}_{\mathcal{R}})\} &= -\frac{1}{2} \log\{\det(\text{diag}(\{\mathbf{D}_s\}_{s \in \mathcal{M}}) + \mathbf{H}_1(\boldsymbol{\Sigma} \otimes \mathbf{V}^*) \mathbf{H}_1^\top)\} - \\ &\quad \frac{1}{2} \{\boldsymbol{\mu}_{\mathcal{M}}^\top (\text{diag}(\{\mathbf{D}_s\}_{s \in \mathcal{M}}) + \mathbf{H}_1(\boldsymbol{\Sigma} \otimes \mathbf{V}^*) \mathbf{H}_1^\top)^{-1} \boldsymbol{\mu}_{\mathcal{M}}\} , \\ \boldsymbol{\mu}_{\mathcal{M}} &= \mathbf{H}_1 \text{vec}(\boldsymbol{\mu}^*) + \mathbf{H}_2 \text{vec}(\mathbf{Y}_{\mathcal{R}}) , \end{aligned} \quad (\text{S.6})$$

then we can use the likelihood and (S.1) to conduct MCMC algorithm for $\boldsymbol{\Sigma}$.

Since $\boldsymbol{\Sigma}$ is positive-definite, we represent $\boldsymbol{\Sigma}$ through $\mathbf{L}\mathbf{L}^\top$ and update \mathbf{L} in the MCMC chain instead. The MCMC update requires transforming the prior by the Jacobian $2^q \prod_{i=1}^q \mathbf{L}_{ii}^{q-i+1}$ to account for the map between \mathbf{L} and $\boldsymbol{\Sigma}$. Benefit from an informative prior $\boldsymbol{\Sigma} | \mathbf{Y}_{\mathcal{R}}$, we can estimate the covariance matrix of the posterior distribution of elements in \mathbf{L} through $\boldsymbol{\Sigma} | \mathbf{Y}$, and design a Gaussian distribution with a covariance matrix equals 2.38² times the estimated covariance matrix as the proposal distribution. The Cholesky decomposition of $E(\boldsymbol{\Sigma} | \mathbf{Y}_{\mathcal{R}}) = \boldsymbol{\Psi} / (\nu^* - q - 1)$ also serves as a good initial value for \mathbf{L} .

The posterior inference of $\boldsymbol{\beta}$ is more straightforward after obtaining the samples of $\boldsymbol{\Sigma} | \mathbf{Y}_{\mathcal{R}}, \{\mathbf{y}(\mathbf{s})_{os}\}_{s \in \mathcal{M}}$. We formulate $\boldsymbol{\beta} | \boldsymbol{\Sigma}, \mathbf{Y}_{\mathcal{R}} | \boldsymbol{\beta}, \boldsymbol{\Sigma}$ and $\{\mathbf{y}(\mathbf{s})_{os}\}_{s \in \mathcal{M}} | \boldsymbol{\beta}, \boldsymbol{\Sigma}$ as the following augmented linear system,

$$\underbrace{\begin{bmatrix} \text{vec}(\mathbf{D}_{\mathcal{R}}^{-\frac{1}{2}}(\mathbf{I} - \mathbf{A}_{\mathcal{R}})\mathbf{Y}_{\mathcal{R}}) \\ \{\mathbf{y}(\mathbf{s})_{os}\}_{s \in \mathcal{M}} - \mathbf{H}_2 \text{vec}(\mathbf{Y}_{\mathcal{R}}) \\ \text{vec}(\mathbf{L}_r^{-1} \boldsymbol{\mu}_{\boldsymbol{\beta}}) \end{bmatrix}}_{\mathbf{Y}^*} = \underbrace{\begin{bmatrix} \mathbf{I}_q \otimes \mathbf{D}_{\mathcal{R}}^{-\frac{1}{2}}(\mathbf{I} - \mathbf{A}_{\mathcal{R}})\mathbf{X}_{\mathcal{R}} \\ \mathbf{H}_1 \\ \mathbf{I}_q \otimes \mathbf{L}_r^{-1} \end{bmatrix}}_{\mathbf{X}^*} \underbrace{\begin{bmatrix} \boldsymbol{\beta}_1 \\ \vdots \\ \boldsymbol{\beta}_q \end{bmatrix}}_{\text{vec}(\boldsymbol{\beta})} + \underbrace{\begin{bmatrix} \boldsymbol{\eta}_1 \\ \boldsymbol{\eta}_2 \\ \boldsymbol{\eta}_3 \end{bmatrix}}_{\boldsymbol{\eta}} , \quad (\text{S.7})$$

where $\mathbf{A}_{\mathcal{R}}$ and $\mathbf{D}_{\mathcal{R}}$ are the $\mathbf{A}_{\rho k}$ and $\mathbf{D}_{\rho k}$ defined in Section III with $\rho_{\psi_k}(\mathbf{s}, \mathbf{s}')$ replaced by $\rho_{\psi}(\mathbf{s}, \mathbf{s}') + (\alpha^{-1} - 1)\delta_{\mathbf{s}=\mathbf{s}'}$ and \mathcal{S} replaced by \mathcal{R} , $\boldsymbol{\eta}$ follows a zero-centered Gaussian distribution with covariance matrix

$$\mathbf{V}_{\boldsymbol{\eta}} = \begin{bmatrix} \boldsymbol{\Sigma} \otimes \mathbf{I}_{\mathcal{R}} & \mathbf{0} & \mathbf{0} \\ \mathbf{0} & \text{diag}(\{\boldsymbol{\Sigma}_{[os,os]}\}_{s \in \mathcal{M}}) & \mathbf{0} \\ \mathbf{0} & \mathbf{0} & \boldsymbol{\Sigma} \otimes \mathbf{I}_p \end{bmatrix} . \quad (\text{S.8})$$

The posterior distribution of $\text{vec}(\boldsymbol{\beta}) | \boldsymbol{\Sigma}, \mathbf{Y}_{\mathcal{R}}, \{\mathbf{y}(\mathbf{s})_{os}\}_{s \in \mathcal{M}}$ follows $\text{MVN}(\boldsymbol{\mu}_{\boldsymbol{\beta}}^*, \mathbf{V}_{\boldsymbol{\beta}}^*)$ with

$$\mathbf{V}_{\boldsymbol{\beta}}^* = (\mathbf{X}^{*\top} \mathbf{V}_{\boldsymbol{\eta}}^{-1} \mathbf{X}^*)^{-1} , \boldsymbol{\mu}_{\boldsymbol{\beta}}^* = \mathbf{V}_{\boldsymbol{\beta}}^* (\mathbf{X}^{*\top} \mathbf{V}_{\boldsymbol{\eta}}^{-1} \mathbf{Y}^*) . \quad (\text{S.9})$$

The posterior prediction over unobserved and misaligned locations Taking \mathcal{R} as the reference set, the full conditional posterior distribution of a new location \mathbf{u} is

$$\mathbf{y}(\mathbf{u}) \mid \mathbf{Y}_{\mathcal{R}}, \boldsymbol{\Sigma}, \boldsymbol{\beta} \sim \text{MVN}(\mathbf{x}(\mathbf{u})^\top \boldsymbol{\beta} + \tilde{\mathbf{A}}_{\mathbf{u}}^\top [\mathbf{Y}_{\mathcal{R}} - \mathbf{X}_{\mathcal{R}} \boldsymbol{\beta}], \tilde{\mathbf{D}}_{\mathbf{u}} \boldsymbol{\Sigma}), \quad (\text{S.10})$$

where $\tilde{\mathbf{A}}_{\mathbf{u}}$ is a $n_{\mathcal{R}} \times 1$ vector whose i -th element is zero if $\mathbf{s}_i \notin N_m(\mathbf{u})$. Define the index of nonzero elements in $\tilde{\mathbf{A}}_{\mathbf{u}}$ as $\text{Pa}[\mathbf{s}]$, then

$$\begin{aligned} \tilde{\mathbf{A}}_{\mathbf{u}}[\text{Pa}[\mathbf{u}]] &= \{\mathcal{K}(\mathbf{u}, N_m(\mathbf{u}))[\mathcal{K}(N_m(\mathbf{u}), N_m(\mathbf{u})) + (\alpha^{-1} - 1)\mathbf{I}_m]^{-1}\}^\top, \\ \tilde{\mathbf{D}}_{\mathbf{u}} &= \alpha^{-1} - \tilde{\mathbf{A}}_{\mathbf{u}}[\text{Pa}[\mathbf{u}]]^\top \mathcal{K}(N_m(\mathbf{u}), \mathbf{u}). \end{aligned} \quad (\text{S.11})$$

For $\mathbf{s} \in \mathcal{M}$, label the index of unobserved responses at \mathbf{s} by us , by the definition of NNGP,

$$\mathbf{y}(\mathbf{s})_{us} \mid \mathbf{Y}_{\mathcal{R}}, \{\mathbf{y}(\mathbf{s})_{os}\}_{\mathbf{s} \in \mathcal{M}}, \boldsymbol{\Sigma}, \boldsymbol{\beta} = \mathbf{y}(\mathbf{s})_{us} \mid \mathbf{Y}_{\mathcal{R}}, \mathbf{y}(\mathbf{s})_{os}, \boldsymbol{\Sigma}, \boldsymbol{\beta} \quad (\text{S.12})$$

follows a Gaussian distribution with mean $\text{E}\{\mathbf{y}(\mathbf{s}) \mid \mathbf{Y}_{\mathcal{R}}\}_{us} - \boldsymbol{\Sigma}_{[us,os]} \boldsymbol{\Sigma}_{[os,os]}^{-1} \{\mathbf{y}(\mathbf{s})_{os} - \text{E}\{\mathbf{y}(\mathbf{s}) \mid \mathbf{Y}_{\mathcal{R}}\}_{os}\}$ and covariance matrix $\tilde{\mathbf{D}}_{\mathbf{s}}(\boldsymbol{\Sigma}_{[us,us]} - \boldsymbol{\Sigma}_{[us,os]} \boldsymbol{\Sigma}_{[os,os]}^{-1} \boldsymbol{\Sigma}_{[os,us]})$ where $\text{E}\{\mathbf{y}(\mathbf{s}) \mid \mathbf{Y}_{\mathcal{R}}\} = \mathbf{x}(\mathbf{s})^\top \boldsymbol{\beta} + \tilde{\mathbf{A}}_{\mathbf{s}}^\top [\mathbf{Y}_{\mathcal{R}} - \mathbf{X}_{\mathcal{R}} \boldsymbol{\beta}]$. The following gives the detailed algorithm:

Algorithm 2: Obtaining inference of $\{\boldsymbol{\beta}, \boldsymbol{\Sigma}\}$ and predictions for conjugate multivariate response NNGP with misalignment.

1. Obtain $\boldsymbol{\mu}^*$, \mathbf{V}^* , $\boldsymbol{\Psi}^*$ and ν^* defined in (III.3) in $\boldsymbol{\Sigma} \mid \mathbf{Y}_{\mathcal{R}} \sim \text{IW}(\boldsymbol{\Psi}^*, \nu^*)$.
The reader may refer to Section 2 and step 1 of Algorithm 1 in Zhang et al. (2020) for a more detailed algorithm.
2. Generate posterior samples of $\boldsymbol{\Sigma} \mid \mathbf{Y}_{\mathcal{R}}, \{\mathbf{y}(\mathbf{s})_{os}\}_{\mathbf{s} \in \mathcal{M}}$ through MCMC algorithm.
 - (a) Take the Cholesky decomposition of $E(\boldsymbol{\Sigma} \mid \mathbf{Y}_{\mathcal{R}})$ as the starting point $\mathbf{L}^{(0)}$ of the MCMC chains
 - (b) Design proposal distribution for elements of $\mathbf{L}^{(l)}$ as a multivariate Gaussian with 2.38² times the covariance estimated from $\text{IW}(\boldsymbol{\Psi}^*, \nu^*)$
 - (c) Construct $\mathbf{L}_{\mathbf{s}}$ and $\mathbf{D}_{\mathbf{s}}$ for $\mathbf{s} \in \mathcal{M}$ as described in (S.2) $\mathcal{O}(n_m m^3)$
 - (d) Construct $\mathbf{H}_1, \mathbf{H}_2$ in (S.4) and calculate $\mu_{\mathcal{M}}$ in (S.6) $\mathcal{O}(n_m m^2)$
 - (e) For l in $1 : L$
 - i. Propose new $\boldsymbol{\Sigma}^* = \mathbf{L}^* \mathbf{L}^{*\top}$ based on $\boldsymbol{\Sigma}^{(l-1)} = \mathbf{L}^{(l)} \mathbf{L}^{(l)\top}$
 - ii. Calculate the likelihood of the new proposed $\boldsymbol{\Sigma}^*$ and $\boldsymbol{\Sigma}^{(l)}$ given $\mathbf{F}^{(l)}$
 - Obtain the Cholesky decomposition $\mathbf{L}_{\text{update}}$ of $\mathbf{V}_{\text{update}}$ in (S.5) $\mathcal{O}(p^2 q^2 n_m)$
 - Generate $u = \mathbf{L}_{\text{update}}^{-1} \mathbf{H}_1 \text{diag}(\{\mathbf{D}_{\mathbf{s}}^{-1}\}_{\mathbf{s} \in \mathcal{M}}) \mu_{\mathcal{M}}$ $\mathcal{O}(pq^2 n_m)$
 - Calculate log-likelihood $l(\boldsymbol{\Sigma} \mid \mathbf{Y}_{\mathcal{R}}, \{\mathbf{y}(\mathbf{s})_{os}\}_{\mathbf{s} \in \mathcal{M}})$ through $\mathcal{O}(n_m)$

$$l(\boldsymbol{\Sigma} \mid \mathbf{Y}_{\mathcal{R}}) - \frac{1}{2} (\log \det(\mathbf{V}_{\text{update}}) + \log \det(\mathbf{V}_{pr}) - \sum_{\mathbf{s} \in \mathcal{M}} \log \det(\mathbf{D}_{\mathbf{s}}) + \mu_{\mathcal{M}}^\top \text{diag}(\{\mathbf{D}_{\mathbf{s}}^{-1}\}_{\mathbf{s} \in \mathcal{M}}) \mu_{\mathcal{M}} - u^\top u)$$
 - Add the log of the Jacobian $2^q \prod_{i=1}^q \mathbf{L}_{ii}$ to the log-likelihood from last step with $\boldsymbol{\Sigma} = \mathbf{L} \mathbf{L}^\top$
 - iii. Accept the new $\boldsymbol{\Sigma}^*$ as $\boldsymbol{\Sigma}^{(l)}$ with the probability of the ratio of the likelihood of $\boldsymbol{\Sigma}^*$ and $\boldsymbol{\Sigma}^{(l)}$. Let $\boldsymbol{\Sigma}^{(l)} = \boldsymbol{\Sigma}^{(l-1)}$ when the new proposal is rejected.
3. Generate posterior samples of $\boldsymbol{\beta}$
 - (a) Construct $\mathbf{A}_{\mathcal{R}}$ and $\mathbf{D}_{\mathcal{R}}$ in (S.7) $\mathcal{O}(n_r m^3)$
 - (b) Construct \mathbf{X}^* and \mathbf{Y}^* in (S.7) $\mathcal{O}(n_r(m+1)(p+q))$
 - (c) For each $\boldsymbol{\Sigma}^{(l)}$ after burn-in
 - i. Construct \mathbf{V}_η in (S.8) and $\mathbf{V}_{\boldsymbol{\beta}}^*, \boldsymbol{\mu}_{\boldsymbol{\beta}}^*$ in (S.9) $\mathcal{O}((p+q)q^2 n)$
 - ii. Generate $\text{vec}(\boldsymbol{\beta}^{(l)})$ from $\text{MVN}(\boldsymbol{\mu}_{\boldsymbol{\beta}}^*, \mathbf{V}_{\boldsymbol{\beta}}^*)$

4. Generate posterior predictive samples of unobserved responses on \mathcal{U} and \mathcal{M} .

- (a) Obtain $\tilde{\mathbf{A}}_{\mathbf{u}}, \tilde{\mathbf{D}}_{\mathbf{u}}$ in (S.11) for all $\mathbf{u} \in \mathcal{U}$. $\mathcal{O}(n'm^3)$
- (b) For each pair of $\boldsymbol{\beta}^{(l)}, \boldsymbol{\Sigma}^{(l)}$
 - i. Generate $\mathbf{y}(\mathbf{u}) \mid \boldsymbol{\beta}^{(l)}, \boldsymbol{\Sigma}^{(l)}, \mathbf{Y}_{\mathcal{R}}$ for $\mathbf{u} \in \mathcal{U}$ through (S.10) $\mathcal{O}(q^2n')$
 - ii. Generate $\mathbf{y}(\mathbf{s})_{is} \mid \boldsymbol{\beta}^{(l)}, \boldsymbol{\Sigma}^{(l)}, \mathbf{y}(\mathbf{s})_{os}$ for $\mathbf{s} \in \mathcal{M}$ through (S.12) $\mathcal{O}(q^2n_m)$

We estimate the hyper-parameter set $\{\psi, \alpha\}$ through Algorithm 3 in Zhang et al. (2020), where in step 1 we use \mathcal{S}_{-k} to denote the location of \mathcal{R} without \mathcal{S}_k .

S.4. MAPS OF PREDICTIONS FOR 10 RESPONSES OF THE FACTOR BLMC MODEL IN REAL DATA ANALYSIS

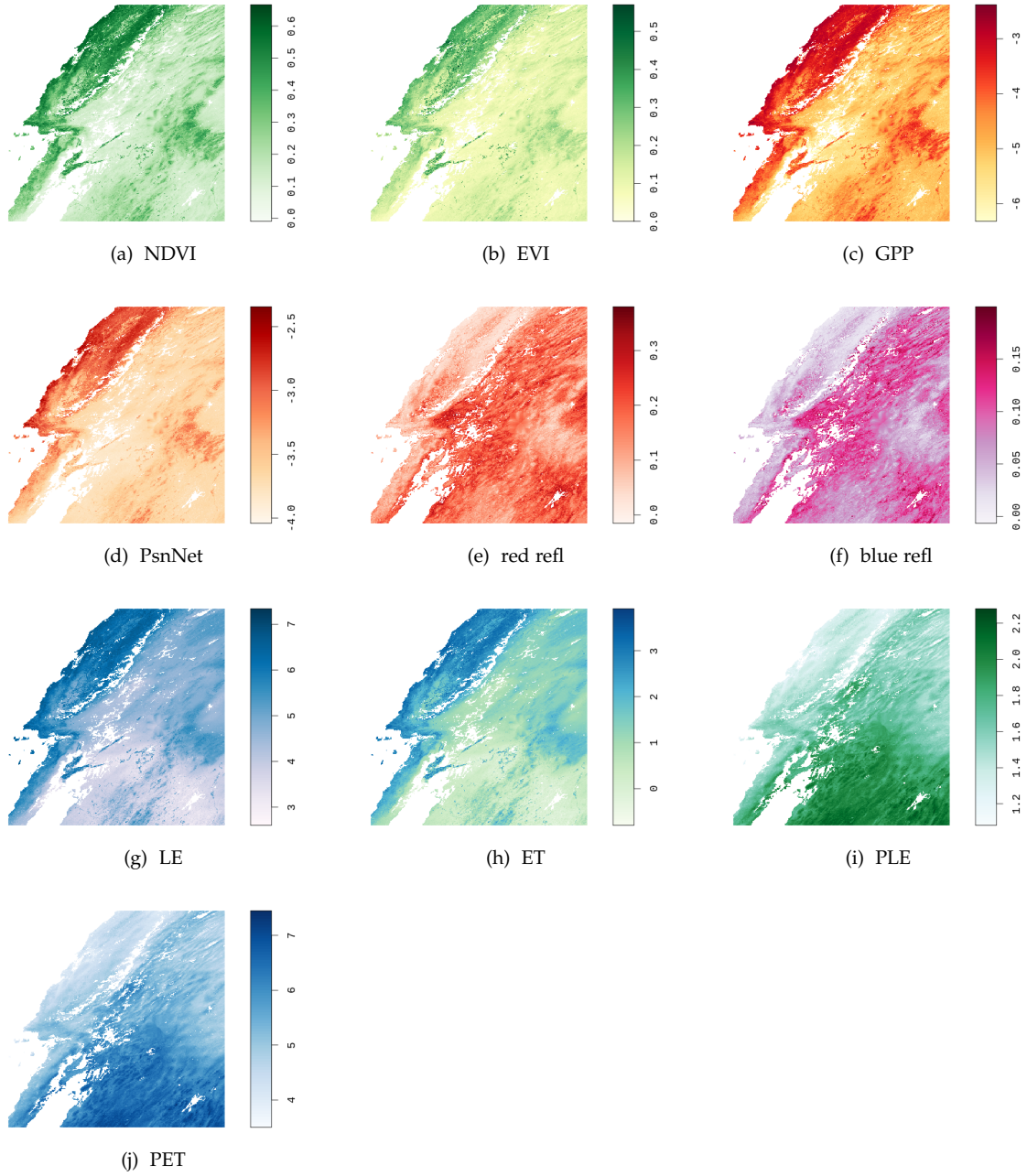


Figure 3: Maps (a)-(j) of predicted value on 1,020,000 observed locations for 10 variables in Section V. The deeper the color, the higher the value. Some variables are transformed for better model fitting. All values are estimated by posterior mean. Each map has its own color scale.